Applied Geochemistry 190 (2025) 106488

Contents lists available at ScienceDirect

Applied Geochemistry

journal homepage: www.elsevier.com/locate/apgeochem

Coupling of Fe and N cycles by nitrate-reducing Fe(II)-oxidizing microorganisms in the tidal sediments of an extreme acidic river (Río Tinto, Spain)

Martina Bottaro [a], Sergey Abramov [b], Ricardo Amils [c], Adrian Martinez-Bonilla [c], Laurel ThomasArrigo [d], Daniel Straub [e], Muammar Mansor [a], Sara Kleindienst [b], Andreas Kappler [a,f,*]

[a] Geomicrobiology, Department of Geosciences, University of Tübingen, Germany
[b] Department of Environmental Microbiology, Institute for Sanitary Engineering, Water Quality and Solid Waste Management (ISWA), University of Stuttgart, Germany
[c] Centro de Biología Molecular Severo Ochoa (CSIC-UAM), Universidad Autónoma de Madrid, Madrid, Spain
[d] Environmental Chemistry, Institute of Chemistry, University of Neuchatel, Switzerland
[e] Quantitative Biology Center (QBiC), University of Tübingen, Germany
[f] Cluster of Excellence: EXC 2124: Controlling Microbes to Fight Infection, Tübingen, Germany

ARTICLE INFO

Editorial handling by: Dr. Yongfeng Jia

Keywords:
Río Tinto estuarian sediments
Geochemical depth profiles
Fe cycling
NRFeOx processes
Microbial community

ABSTRACT

Río Tinto (Huelva, Spain) is an acid rock drainage-affected fluvial estuarine system where Fe(II)-oxidizing microorganisms were shown to be active both in the water column and in the top sediment layer, contributing to Fe mineral accumulation (up to 30 % of dry sediment weight) in the estuarian sediment. However, it is still unknown if the Fe(II)-oxidizing microorganisms thriving in the upper sediment layer are also capable of using nitrate present in the river (0.05–0.5 mM) as electron acceptor. We performed sediment incubations amended with either lactate, acetate-/NO_3^--/Fe_{aq}^{2+} or NO_3^-/Fe_{aq}^{2+} to evaluate Fe-cycling processes and, specifically, if nitrate reduction coupled to Fe(II) oxidation (NRFeOx) can occur in the sediment under anoxic conditions. Geochemical data showed that in the NO_3^--/Fe_{aq}^{2+}-amended setup, NO_3^- (from 1.5 to 0 mM), Fe_{aq}^{2+} (from 1.5 to 0 mM) and pH (from 6.0 to 5.4) decreased, while the poorly crystalline Fe(III) mineral pool increased by 6.9 % during 114 days of incubation. In the acetate-/NO_3^--/Fe_{aq}^{2+}-amended setup, nitrate reduction rates (0.31 mM NO_3^-/day) were 10 times faster compared to the NO_3^--/Fe_{aq}^{2+}-amended setup (0.03 mM NO_3^-/day). pH and poorly crystalline Fe(II) mineral content increased due to Fe(III) reduction after amendment with only lactate (0.26 ± 0.03 mM Fe_{aq}^{2+}/day) but also after amendment with acetate-/NO_3^--/Fe_{aq}^{2+} (0.16 ± 0.02 mM Fe_{aq}^{2+}/day) suggesting that acetate-stimulated Fe(III) reduction superimposed Fe(II) oxidation coupled to nitrate reduction. Sequencing data showed that upon addition of nitrate, members of the genus *Rhodanobacter* increased by ~10 % in relative DNA-based 16S rRNA gene abundances in both acetate-/NO_3^--/Fe_{aq}^{2+}- and NO_3^--/Fe_{aq}^{2+}-amended setups. However, the *Rhodanobacter* RNA-based 16S rRNA relative gene abundance was higher in the acetate-/NO_3^--/Fe_{aq}^{2+}-amended setup (11.15 ± 2.24 %) than in the NO_3^--/Fe_{aq}^{2+}-amended one (5.40 ± 0.31 %). Combining geochemical and sequencing data obtained from anoxic sediment incubations, we conclude that NRFeOx processes, potentially catalyzed by the genus *Rhodanobacter*, can play a role in Fe cycling in this extreme acid rock drainage affected river, under low organic carbon (OC) conditions. At higher OC levels, NRFeOx microorganisms seem to become more active but their net effects on Fe(II) oxidation can be diminished due to the simultaneous activity of Fe(III)-reducers.

1. Introduction

The Río Tinto is a 92 km long river located in southwest Spain discharging into the Gulf of Cadiz (Atlantic Ocean) characterized by orange-red colored waters and sediments observed already before the settlement of Roman colonies and their first mining activities 5000 years

* Corresponding author. Geomicrobiology, Department of Geosciences, University of Tübingen, Germany.
E-mail address: andreas.kappler@uni-tuebingen.de (A. Kappler).

https://doi.org/10.1016/j.apgeochem.2025.106488
Received 30 November 2024; Received in revised form 21 May 2025; Accepted 28 June 2025
Available online 1 July 2025

ago (Fernández-Remolar et al., 2005). This unique coloration originates from the high Fe concentrations (up to 360 mM) and heavy metal (HM) loads (González-Toril et al., 2003), which remain dissolved in the water due to the extremely acidic conditions (pH ~2.2) (López-Archilla et al., 2001). Once saturation is reached, dissolved Fe^{3+} precipitates as minerals forming Fe(III) hydroxysulfates (mainly jarosite and schwertmannite) and Fe(III) (oxyhydr)oxides (such as ferrihydrite, hematite and goethite) (Bedini et al., 2022; Sobron et al., 2014; Fernández-Remolar and Knoll, 2008). The reason for Río Tinto's unique geochemistry lies in the geology of the Iberian Pyrite Belt area, where the river originates, considered to be one of the largest deposit of metal sulfides in the Earth's crust. It has been shown that the peculiar geochemistry of the river is the result of microbial activity occurring in the subsurface. Diverse chemolithotrophic microorganisms are able to couple C, H, N, S and Fe geochemical cycles (Amils et al., 2023) and act as an underground bioreactor responsible for the bioleaching of metal sulfides (Vera et al., 2013) leading to acidification and high concentrations of dissolved HMs, Fe and sulfate in the upper part of the river. In addition to these natural processes, past and ongoing mining activities expose sulfide waste deposits to the air (Olías and Nieto, 2015), further exacerbating the already extreme conditions of the river.

The geochemistry of the river becomes even more complex and unique when the acidic water mixes with the saltwater due to tidal influence. The saltwater influx causes a drastic change in the geochemistry of the last 50 km (up to the city of Niebla) of the river by increasing the pH of the water up to circumneutral conditions (Olías et al., 2020), thus, affecting the solubility of Fe and HMs in the river water on a daily basis. The precipitation of Fe(III) (oxyhydr)oxides in the presence of O_2 at circumneutral pH is a well-known abiotic process (Stumm and Morgan, 1996) but can also be biotically mediated by planktonic microaerophilic Fe(II)-oxidizing microorganisms such as *Mariprofundus* and *Marinobacter*, which are neutrophilic bacteria (active during high tide), and by *Acidihalobacter*, an acidophilic halotolerant bacterium (active during low tide) thriving in the upper estuary of the river (Abramov et al., 2021). Both biotic and abiotic Fe(II) oxidation pathways contribute to the formation of suspended particulate matter (SPM) composed of microbial cells, Fe(III) minerals such as schwertmannite and ferrihydrite, and co-sorbed HMs. These components aggregate and settle over time to the river bottom and floodplains, forming a thick reddish sediment layer enriched in Fe(III) minerals, organics and HMs (Abramov et al., 2020).

Within this top reddish sediment layer, Fe mineral transformation is promoted by diurnal fluctuations in pH, salinity and redox conditions induced by tidal activity. Within the sediment, Fe(III)-reducing microorganisms, sulfate-reducing bacteria (SRB) and microaerophilic Fe(II)-oxidizing microorganisms are the main contributors to the Fe cycle (Abramov et al., 2021). However, one metabolism that has been overlooked is nitrate reduction coupled to the oxidation of dissolved Fe^{2+} or Fe(II)-bearing minerals (NRFeOx). Nitrate is in fact present in the water and the dissolved concentrations (0.05–0.5 mM) can vary depending on the season and high/low tidal activity (Abramov et al., 2020). NRFeOx is a well-known process widespread in many different environments such as rice paddy soils (Tong et al., 2023), freshwater lake sediments (Li et al., 2023), saltwater sediments (Huang et al., 2022a), groundwaters (Smith et al., 2017) and wastewater sludges (Nielsen and Nielsen, 1998). This process occurs under anoxic conditions, where NRFeOx microorganisms are able to use inorganic C such as CO_2 (Huang et al., 2021) or organic compounds such as acetate (Muehe et al., 2009) as carbon sources.

Most of the previous studies at the Río Tinto focused on the characterization of the microbial community in the subsurface (Amils et al., 2023; Sánchez-Andrea et al., 2012) and the upper part of the river where the pH is constantly acidic (González-Toril et al., 2003; Sánchez-Andrea et al., 2011). Particularly, Amils et al. (2023) detected NRFeOx microorganisms such as *Pseudomonas* and *Acidovorax* in the subsurface of the Iberian Pyrite Belt (where the Río Tinto originates) suggesting that NRFeOx could contribute to the underground Fe(II) oxidation. However, much less is known about how the microbial community influences the Fe cycle in the anoxic sediment of the upper estuary, where extreme pH and salinity fluctuations occur daily. To the best of our knowledge, NRFeOx microorganisms have not been yet studied in such saline and simultaneously extremely acidic environments. Furthermore, an integrated geochemical, mineralogical, and *in-situ* microbial community characterization of these sediments is still missing, limiting our understanding of NRFeOx processes under such extreme conditions. Therefore, studying NRFeOx in the estuarian sediment of the Río Tinto could i) identify the microorganisms capable of using nitrate to enzymatically oxidize Fe(II) and produce Fe(III) minerals with co-sorbed HMs, potentially acting as an *in-situ* natural bio-remediation process within the anoxic sediment of the Río Tinto, ii) provide an understanding of the enzymatic and abiotic pathways involved in NRFeOx by enriching and isolating new model organisms, and iii) set the basis for future bioengineering applications for the simultaneous removal of NO_3^- and HMs in AMD-like contaminated water bodies. Therefore, based on the knowledge gaps mentioned above, the aims of this work were i) to identify mineralogical and hydrogeochemical parameters of the sediments collected from the upper estuary of the river to assess the availability of electron donors and acceptors required for NRFeOx microorganisms, ii) to address if nitrate reduction can be coupled to Fe(II) oxidation in sediment microcosm experiments with or without the addition of C sources, iii) to identify the microorganisms capable of NRFeOx both in the *in-situ* community and in the microcosm experiments.

2. Materials and methods

2.1. Field site and sampling procedure

River water and 6 sediment cores were collected between the September 30, 2022 and October 03, 2022 (dd.mm.yyyy) from the upper estuary of the Río Tinto river near the city of San Juan Del Puerto. Salinity (WTW; TetraCon92), pH and temperature (WTW; SenTrix), oxygen saturation (WTW; FDO925) of river water samples were simultaneously monitored (WTW; Multi 3430) *in-situ* from the river tidal flat (37°18′39.0″N 6°49′23.0″W) between 11:30 a.m. and 4:30 p.m. on the 01.10.2022 to assess hydrogeochemical fluctuations during high and low tidal activity (Fig. S1). At the same time, triplicate river water samples were filtered with 0.45-µm-pore-size membrane filters (HAWG050S6; Merck) and stored at 4 °C in the dark. The samples were used for dissolved organic carbon (DOC) analysis by pre-acidification with 2 M HCl (to remove inorganic carbon) followed by combustion at 750 °C (Elemental Analyzer, multi N/C 2100S, Analytik Jena GmbH, Germany). Fatty acid concentrations of the filtered samples were quantified by High Performance Liquid Chromatography (HPLC; class VP with a refractive index detector [RID] 10 A and photo-diode array detector SPD-M10A VP detectors; Shimadzu, Japan). Additionally, dissolved NH_4^+, NO_3^- and NO_2^- were quantified by a segmented flow analyzer (AutoAnalyzer3, SEAL Analytical, Germany) equipped with a dialysis membrane for Fe removal to prevent side reactions during measurement. Filtered river water samples were stabilized with 1 M HCl for Fe speciation analysis by ferrozine assay (Stookey, 1970) and with 2 % (v/v) analytical grade HNO_3 for total element analysis by inductively coupled plasma mass spectrometry (ICP-MS Agilent 7900). Six different cores were collected during a low tidal event (3:00 pm) using 60 cm long PVC liners (90 cm diameter, UWITEC GmbH, Germany) along the river tidal flat in a non-vegetated area (37°18′37.2″N 6°49′20.7″W for cores 1, 2, 4, and 5 collected within a 10 m^2 area) and shrub vegetated area (37°18′38.7″N 6°49′23.7″W for cores 3 and 6 collected within a 5 m^2 area). The PVC cores were washed three times with 80 % ethanol, subsequently rinsed three times with sterile double-deionized water (DDI, Green Pure Pro UV, >18,2 MΩ/cm, ThermoFisher Scientific) and sealed from both ends with butyl stoppers once dried until core collection. Butyl stoppers were washed with 80 % ethanol and boiled three times in DDI. Holes for microrhizon insertion (0.4 cm diameter) and

sediment collection (1 cm diameter) were pre-drilled in the PVC cores to depth resolution of 5 cm and sealed with gas-tight tape prior to ethanol and DDI washing. Porewater samples were collected in the field immediately after the extrusion of each core by cutting the gas-tight tape (that was sealing the pre-drilled hole) and inserting microrhizons (0.15 μm as effective pore size; Rhizosphere Research Products, Netherlands). Each microrhizon was attached to 10 mL gas-tight syringes via a bivalve connector. We ensured anoxic porewater collection by flushing each syringe (and the attached bivalve connector) three times with N_2. The syringes and bivalve connectors were then immediately attached to the inserted microrhizons and all were evacuated four times to ensure even porewater suction. Porewater collection was initiated by opening all the bivalves simultaneously. All the microrhizons were stored in N_2-flushed Schott bottles prior to insertion in the sediment core. The cores were kept in a vertical position during porewater and sediment sampling. For each porewater sample, the first collected milliliter was used for pH measurement. An additional aliquot (1 ml) was immediately stabilized with 1 M HCl for Fe speciation analysis and stored in the dark at 4 °C. The rest of the collected porewater was directly injected from the gas-tight syringe into sterile anoxic serum bottles and stored in the dark at 4 °C for inorganic N species, DOC, fatty acids and total element analysis (all measured as previously described). Correlation analysis between different porewater geochemical parameters were also performed: p values and correlation coefficients (r) were calculated using RStudio 4.4.0 with the Hmisc package. Pairwise Pearson correlation coefficients were calculated using the rcorr() function, which also provided associated p-values for significance testing. The dataset comprised 40 samples, corresponding to 38 degrees of freedom in the correlation calculations. Additionally, sediment samples were collected in triplicate at each depth using a sterile, nitrogen-flushed 3 ml syringes with pre-cut tip. The cut syringe was inserted into the pre-cut PVC liner and the sediment was collected at the same depth as the porewater samples. The sediment was then directly extruded under a flame into sterile anoxic (flushed with N_2) serum bottles, crimped, immediately frozen using dry ice and kept at −80 °C prior to DNA and RNA extraction or stored in the dark at 4 °C for mineralogical analysis. Bulk sediment from the top oxic-reddish layer was collected from the river tidal flat (where cores 5 and 6 were sampled) using sterile spatulas and stored oxically (at 4 °C in the dark) in a sterile Schott bottle for microcosm experiments (section 2.3).

2.2. Mineralogical analysis of sediment samples

Sediment samples collected in the field (as described in section 2.1) were manually homogenized by mixing and dried in the glovebox (100 % N_2 atmosphere) immediately after the field campaign until no further weight loss was observed (2 days). All further steps were performed in triplicate in the glovebox. Two milliliters of anoxic 0.5 M HCl were added to 200 mg of dried sample to target the poorly crystalline Fe mineral phases (Moeslundi et al., 1994). The samples were shaken for 1 h and then centrifuged at 5,300*g* for 10 min. The supernatant was collected, and 1 ml was stabilized with 1 M HCl (1:1) for further Fe speciation analysis. Then, 2 ml of anoxic 6 M HCl were added to the pellet for the determination of more crystalline Fe phases (Roden and Zachara, 1996). During this step, the sediment was shaken for 24 h and the supernatant was sampled as described above, followed by 1:6 dilution with 1 M HCl in order to avoid Fe(II) oxidation by O_2 at extremely acidic conditions (Porsch and Kappler, 2011). Fe(II) and total Fe concentrations were determined immediately after stabilization of the anoxic samples using the ferrozine assay (Stookey, 1970). Speciation and oxidation state of solid-phase Fe for two representative sediment samples was analyzed by bulk Fe K-edge (7112 eV) XAS at the XAFS beamline of ELETTRA (Trieste, Italy). For these analyses, dried samples were pressed into 0.7 cm pellets and sealed with Kapton tape in the glovebox (100 % N_2 atmosphere). X-ray absorption near edge structure (XANES) and extended X-ray absorption fine structure (EXAFS) spectra were recorded in transmission mode at ~80 K using a N_2(l) cooled cryostat. The Si(111) monochromator was calibrated to the first-derivative maximum of the K-edge absorption spectrum of a metallic Fe foil (7112 eV). The foil was continuously monitored to account for small energy shifts (<1 eV) during the sample measurements. Higher harmonics in the beam were eliminated by detuning the monochromator to 30 % of its maximal intensity. Two scans per sample were collected and merged. All spectra were energy calibrated, pre-edge subtracted, and post-edge normalized in Athena (Ravel and Newville, 2005) with the edge energy, E_0, defined as the zero-crossing in the second XANES derivative. To determine spectral contributions from Fe (II) and Fe(III), linear combination fit (LCF) analyses were performed over the energy range −20 to 30 eV (E - E_0) with no constraints. Initial fit fractions (99 ± 1 %) were recalculated to a component sum of 100 %. Linear combination fit (LCF) analyses of k^3-weighted EXAFS spectra were performed in Athena over a k-range of 2–12 $Å^{-1}$ with the E_0 of all spectra and reference compounds set to 7128 eV. To narrow down the number of possible references, each sample was least-squares simulated in Athena (Ravel and Newville, 2005) by calculating all single to five component fits. This approach identified three consistently contributing references (chlorite, schwertmannite, goethite). From there, the number of components included in the fit was successively increased and each additional component was retained in the fit when the NSSR value decreased by at least 10 % and contributed to >5 % of total Fe. References considered are listed in Table S1. No constraints were imposed on the fits, and initial fit fractions were recalculated to a component sum of 100 %.

2.3. Microcosm experiments setup and sampling

The bulk top sediment layer collected during the 2022 field campaign was stored in the dark at 4 °C for 6 months prior to setting up the microcosms. The collected bulk sediment (430 g) was mixed 1:1 with sterile anoxic low-phosphate medium buffered with 22 mM bicarbonate. The content of the low-phosphate medium is shown in the supporting information (Table S2) and the pH of the medium was adjusted to 6 using sterile anoxic 1 M HCl before mixing it with the sediment. All the salts used to prepare the low-phosphate medium were dissolved in DDI water. The obtained slurry was purged with a mixture of N_2/CO_2 for 1 h. The water content of the slurry (50 %) was then quantified. Subsequently, 100-ml serum bottles were filled with the 16 ml of slurry (with constant stirring) and additional 64 ml of low-phosphate medium to obtain a final dry sediment-to-water ratio of 10 %. All the electron donors/acceptors and C sources were added individually to each bottle depending on the setup on the bench by using a N_2 flushed gas-tight syringe under the flame. Each setup had four replicate bottles. Four bottles were amended with 1 mM lactate as $NaC_3H_5O_3$ (referred in the text as lactate-amended setup) for a total of three times after every complete lactate consumption. In four additional bottles (acetate-/NO_3^--/Fe_{aq}^{2+}-amended setup), 0.5 mM acetate (as $C_2H_3NaO_2$), 1.5 mM NO_3^- (as $NaNO_3$) and 2 mM Fe_{aq}^{2+} (as $FeCl_2$) were initially added but only NO_3^- and acetate were re-added three times after full consumption as Fe_{aq}^{2+} was never depleted during the experiment. In the setup where only 1.5 mM of NO_3^- and 2 mM of Fe_{aq}^{2+} were added (NO_3^--/Fe_{aq}^{2+}-amended setup), the pH needed to be increased with 0.5 mM of Na_2CO_3 (anoxic sterile). In the NO_3^--/Fe_{aq}^{2+}-amended setup, NO_3^- was added for a total of three times while Fe_{aq}^{2+} was added for a total of four times after full consumption. Four bottles containing acetate, lactate, NO_3^- and Fe_{aq}^{2+} were additionally amended with NaN_3 to a final concentration of 160 mM (Otte et al., 2018) to inhibit microbial activity and used as abiotic controls. Each preparation step was carried out under sterile conditions (under a flame) while flushing the bottles headspace with N_2/CO_2 gas mixture. All microcosms were incubated at 20 °C in the dark for a maximum of 114 days. All bottles used for the microcosm experiments were briefly exposed to light (1 h) and each bottle was manually shaken during each sampling event (as indicated in Fig. 4). The sampling was

carried in an anoxic glovebox (100 % N_2 atmosphere). At each sampling event, between 1 and 2 ml (depending on the sampling) of the sediment slurry was centrifuged for 10 min at 5,300*g* and the supernatant was collected for determination of NO_2, NO_3^-, total Fe, Fe(II), acetate and lactate, determination of DOC and total dissolved elements by ICP-MS. In the acetate-/NO_3^--/Fe_{aq}^{2+}-amended setup, samples for the ferrozine assay were stabilized with 1 M HCL containing 40 mM sulfamic acid in order to prevent Fe(II) oxidation by nitrite (Schaedler et al., 2018). The pellet remaining after centrifugation was dried anoxically and used for sequential Fe extraction (as described in section 2.2). After each sampling event, the sampled volume was replaced with the same amount of N_2/CO_2 gas mixture. A schematic of the microcosm experiment setups, sampling and all the different amendments/controls can be seen in Picture S1. To determine the microbial community at the beginning of the experiment, three additional bottles were prepared as previously described (without substrates addition) and used to sample 10 ml of slurry for DNA/RNA extraction. At the end of the experiment, 10 ml of slurry were also sampled for each setup in triplicate and immediately frozen and stored at −80 °C until DNA/RNA extraction.

2.4. Microbial community analysis

Simultaneous extraction of total DNA and RNA from the sediment cores and microcosm experiments was performed using a phenol-chloroform extraction protocol (Lueders et al., 2004). The quantity and quality of the extracted DNA and RNA were determined using Qubit (Life Technologies, Carlsbad, CA, USA), NanoDrop (NanoDrop 1000, Thermo Scientific, Waltham, MA, USA) and gel electrophoresis. DNA was digested using the TURBO DNA-free™ Kit to obtain pure RNA samples, followed by reverse transcription to obtain complementary DNA (cDNA) using SuperScript™ III Reverse Transcriptase. The microbial 16S rRNA (gene) was amplified using primers 515F (Parada et al., 2016) and 806R9 (Apprill et al., 2015). Library preparation steps (Nextera, Illumina) and sequencing were performed using Illumina MiSeq sequencing system (Illumina, USA) at the Institute for Medical Microbiology and Hygiene (MGM) of the University of Tübingen. In total 7,329,009 paired-end reads with length 250 bp were obtained for 66 samples (70,964 to 161,214 read pairs per sample, in average 111,045). Data processing, including quality control, reconstruction of sequences and taxonomic annotation was done using nf-core/ampliseq version 2.9.0 (Straub et al., 2020) of the nf-core collection of workflows (Ewels et al., 2020). The pipeline was executed with nextflow v23.10.1 and singularity v3.8.7 (Di Tommaso et al., 2017; Kurtzer et al., 2017). Primers were trimmed using Cutadapt v4.6 (Martin, 2011) and untrimmed sequences were discarded. Less than 27 % of sequences were discarded per sample and 89.8 % of sequences passed the filtering on average. Adapter and primer-free sequences were pooled with DADA2 v1.30.0 (Callahan et al., 2016) to eliminate PhiX contamination, trim reads (forward reads at 225 bp and reverse reads at 55 bp), discard reads with >2 expected errors, correct errors, merge read pairs, and remove PCR chimeras. Ultimately, 11,864 amplicon sequencing variants (ASVs) were obtained across all samples. Between 46 % and 60 % reads per sample (average 57.8 %) were retained. ASVs with length lower than 240 or above 270 bp were removed (16 of 11,864). Taxonomic classification was performed by DADA2 and the database 'Silva 138.1 prokaryotic SSU' (Quast et al., 2013). Of 11,848 ASVs, 188 ASVs designated as mitochondria or chloroplasts were removed within QIIME2 version 2023.7.0 (Bolyen et al., 2019), reducing reads by less than 8 % (average 1.9 %). Finally, 11,660 amplicon sequencing variants (ASVs) with between 35,608 and 79,813 reads (average 56,233) per sample were obtained.

3. Results and discussion

3.1. In-situ Fe mineral composition of the estuarine sediments at different depths

The collected sediment cores showed alternating black and red layers over depths as can be seen in Picture S2. Even though cores 1 and 2 were collected only ~1 m apart from each other, substantial differences in the sediment layering could be observed. In order to understand the changes in Fe minerology between these black and orange layers, sequential extractions targeting Fe phases with different crystallinity were performed (three different cores; see Fig. 1). Results showed that the extractable Fe concentrations (as the sum of Fe extracted sequentially with 0.5 M and 6 M HCl for each depth) within the sediment reached up to 300 mg Fe/g dry sediment (30 wt% Fe). Fe concentrations generally decreased in the deeper sediment layers (Fig. 1C). The high Fe content was overall comparable to values obtained in previous studies (Abramov et al., 2020). Fe(II)/Fe_{tot} values (Fig. 1B), calculated based on acidic Fe extractions, and pH values (Fig. 1A) showed a significant positive correlation for both poorly crystalline (Fe extractable with 0.5 M HCl) and more crystalline (extractable with 6 M HCl) Fe phases (higher Fe (II)/Fe_{tot} ratios at pH ~ 7; the respective correlation coefficients were: $r = 0.64$, $p < 0.0001$ and $r = 0.4$, $p < 0.05$). The data also indicated a negative correlation between poorly crystalline Fe(III) phases and pH (higher Fe(II)/Fe_{tot} ratio at higher pH values; $r = -0.65$, $p < 0.0001$; Fig. S2). Note that the mineralogical data obtained from sequential Fe extractions of three additional sediment cores were also used for the correlation analysis between pH and Fe minerals (shown in Fig. S3).

These mineralogical data suggest that at depths characterized by acidic pH, the sediment was mainly composed of Fe(III) minerals, while, at circumneutral pH, poorly crystalline Fe(II) mineral phases were more abundant. Specifically, Fe extraction data obtained from core 1 at 15 cm depth (pH = 5.7) showed that the Fe(II)/Fe_{tot} ratio for the poorly crystalline Fe phases and more crystalline Fe phases were 0.06 and 0.14, respectively (Fig. 1B). These low Fe(II)/Fe_{tot} values indicated that the sediment was mainly composed of Fe(III) minerals. Mineralogical data obtained by synchrotron-based Fe K-edge EXAFS analysis of the same sediment (Fig. 1D) confirmed the presence of Fe(III) minerals as the only detectable Fe phases, comprising of ferrihydrite (22 %), goethite (37 %), schwertmannite (24 %) and jarosite (17 %). At 10 cm depth (pH 6.3), the Fe(II)/Fe_{tot} ratio for the poorly crystalline Fe phases and the more crystalline Fe phases increased to 0.6 and 0.4, respectively, indicating a higher Fe(II) mineral content compared to 15 cm depth. Fe K-edge EXAFS analysis also confirmed the presence of Fe(II) mineral phases at 10 cm depth (~25 %, matching the results obtained by sequential Fe extraction) including mackinawite (14 %) and chlorite (13 %). Fe(III) minerals were still present as goethite (19 %) and schwertmannite (21 %) while other Fe(III) phases such as lepidocrocite (9 %) and Fe(III) complexed to organic compounds (24 %) were identified. These mineralogical differences between these two sediment layers could also be visually observed (Fig. 1E).

We found that the reddish "oxidized" sediment (at 15 cm depth) was characterized by acidic pH and the presence of mainly Fe(III) minerals whereas the blackish "reduced" sediment (10 cm depth) had higher porewater pH values and higher Fe(II) mineral content. From the obtained mineralogical data it can be concluded that Fe cycling, i.e., oxidation of Fe(II) and reduction of Fe(III), is likely to occur within the estuarian sediment. However, to reveal the main processes driving the formation and transformation of Fe mineral as well as the coupling of the Fe to the N cycle, both river and porewater geochemistry together with the composition and activity of the *in-situ* microbial community needed to be evaluated.

3.2. Hydrogeochemical fluctuations in river water and porewater samples

The monitored hydrogeochemical parameters of the river water

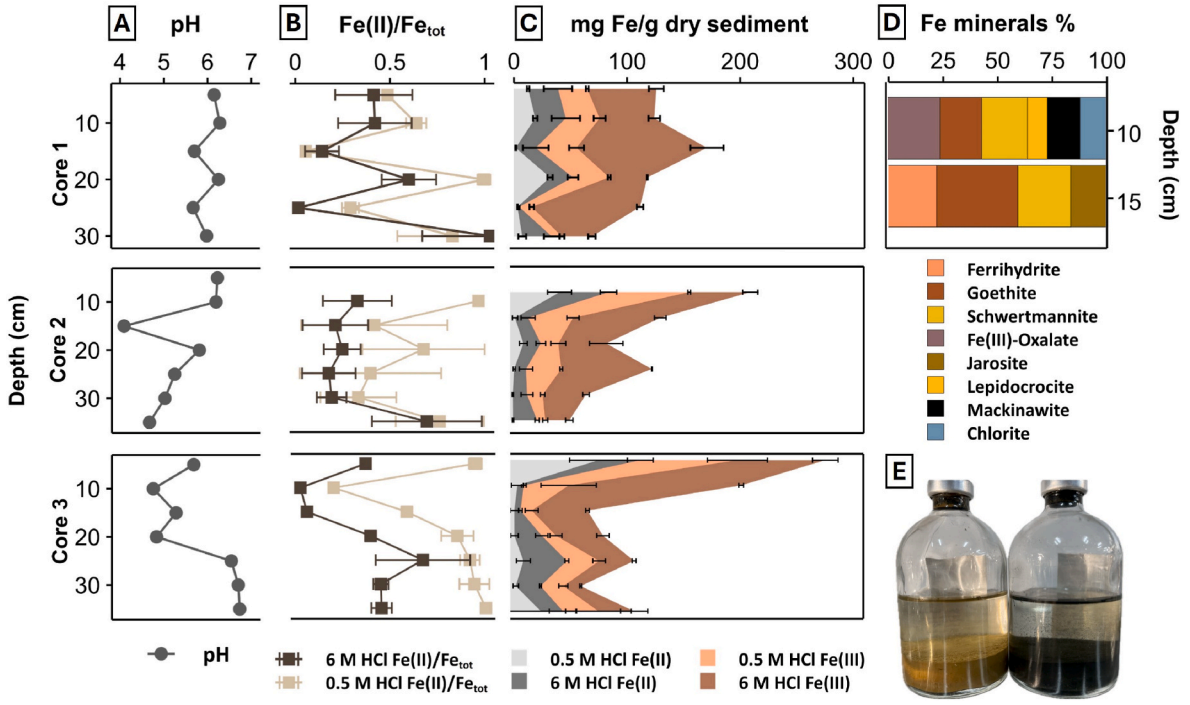

Fig. 1. Geochemical and mineralogical data for sediment cores collected in the upper estuary of the Río Tinto near the city of San Juan Del Puerto (A) pH profile of three representative sediment cores (cores 1, 2 and 3). Porewater geochemical profiles of the same cores and their sampling locations are shown in Fig. 2A. **(B)** Fe(II)/Fe$_{tot}$ ratios based on sequential extraction of poorly crystalline Fe minerals (extractable with 0.5 M HCl) are shown in light brown while crystalline Fe phases (extractable with 6 M HCl) are shown in dark brown. **(C)** Total amount of Fe(III) (shown in light orange for the 0.5 M HCl extraction and in dark orange for the 6 M HCl extraction) and Fe(II) (shown in light grey for the 0.5 M HCl extraction and in dark grey for the 6 M HCl extraction). **(D)** Results of Linear Combination Fitting (LCF) of Fe K-edge EXAFS spectra of sediment collected from core 1 at two different depths (10 and 15 cm). Fe K-edge EXAFS linear combination fit, standards and spectra are shown in Fig. S4. **(E)** Examples of reddish sediment (15 cm depth) and black sediment (10 cm depth) collected from core 1. (For interpretation of the references to color in this figure legend, the reader is referred to the Web version of this article.)

(Fig. S1A) indicated a constant influx of seawater during the sampling event in the late summer. Na concentrations (13 g/L during low tide and 15 g/L during high tide) and salinity values (between 35 g/L during low tide and 40 g/L during high tide) were comparable to seawater values and showed minimal variations during the low tide (at 2:30 p.m.) and high tide (at 1:00 and 5:00 p.m.) events. Total dissolved solids (TDS) decreased during low tide while pH values fluctuated between 7 (high tide) and 5.5 (low tide). The lower TDS concentrations during the low tide were likely due to the decreased SPM formation (as discussed in the introduction) under the more acidic conditions. Total S concentrations (between 1 and 2 g/L) were always high since seawater and the Río Tinto river are both characterized by elevated sulfate concentrations (Olías et al., 2020). Dissolved organic carbon (DOC) values (mean value of 13.6 mg C/L) showed minor fluctuations over time. Dissolved NO_3^- increased during the low tide event (to values up to 2.5 mg/L). Fe_{aq}^{3+} was detected at low concentrations (between 5 and 7 mg/L), while Fe_{aq}^{2+} was below the detection limit, most likely due to the oxic conditions of the river water (average O_2 concentrations and temperature were 13 mg/L and 22 °C, respectively) leading to Fe(II) oxidation and precipitation of Fe(III) minerals (as discussed in the introduction). Such Fe(III) minerals could also have been present in the river water as nanoparticles smaller than 0.22 μm (Mansor et al., 2021; Neil et al., 2016) and therefore detected in the dissolved phase even at circumneutral pH.

Dissolved HMs showed different behavior over time. Zn, Cu and Pb increased (concentrations were 6.9 mg/L, 355 μg/L and 230 μg/L, respectively) whereas Cr and As concentrations were at the lowest during low tide (concentrations were 300 and 5 μg/L, respectively) when the sediment cores were sampled (Fig. S1). Overall, diurnal fluctuations of hydrogeochemical parameters were less pronounced compared to a previous sampling campaign performed in spring (Abramov et al., 2020) due to stronger tidal activity in the late summer months.

We compared the river water geochemistry to geochemical data obtained from porewater samples collected from six different sediment cores during the low tide event. Fig. 2A shows geochemical profiles of three representative cores (core 1 to core 3). The data for 3 additional cores are shown in Fig. S5. Porewater Na concentration (on average 15 g/L), as well as other major cations, did not differ from river water concentrations. However, other hydrogeochemical parameters showed higher fluctuations in the sediment compared to the river water. Porewater samples had significantly lower or higher pH values (depending on the depth) compared to the river water (pH 5.5) during the low tide core sampling event. pH values showed fluctuations of up to 1 or 2 pH units within 5 cm depth (Fig. 2A) and overall ranged from 3.5 to 6.5 within the sediments. Fe_{aq}^{2+} concentrations showed a significant positive correlation with depth (Fig. 2C) and increased up to 0.5 g/L in the deeper sediment layers (Fig. 2B). DOC and NH_4^+ showed significant positive correlations with Fe_{aq}^{2+} (Fig. 2C) and both increased up to 40 mg/L and 19 mg/L, respectively. NO_3^- and lactate were detected at low concentrations (with a maximum of 2.5 and 2.6 mg/L, respectively) in a few porewater samples. Therefore, it was not possible to perform any statistical analysis or show correlations with other geochemical parameters.

The main HMs detected in the sediment porewater were Zn, Cu, Pb and As and their concentrations increased within the sediment up to 8, 2.4, 0.5 and 0.68 mg/L, respectively. Cu and Zn negatively correlated with pH and depth indicating that these elements were probably immobilized at higher pH and deeper within the sediment. Arsenic behaved differently and seemed to be mobilized with increasing pH, depth and Fe_{aq}^{2+} porewater concentrations. The different behavior of Cu, Zn and Pb compared to As, also observed in the river water data, has already been reported in previous publications (Cánovas et al., 2014)

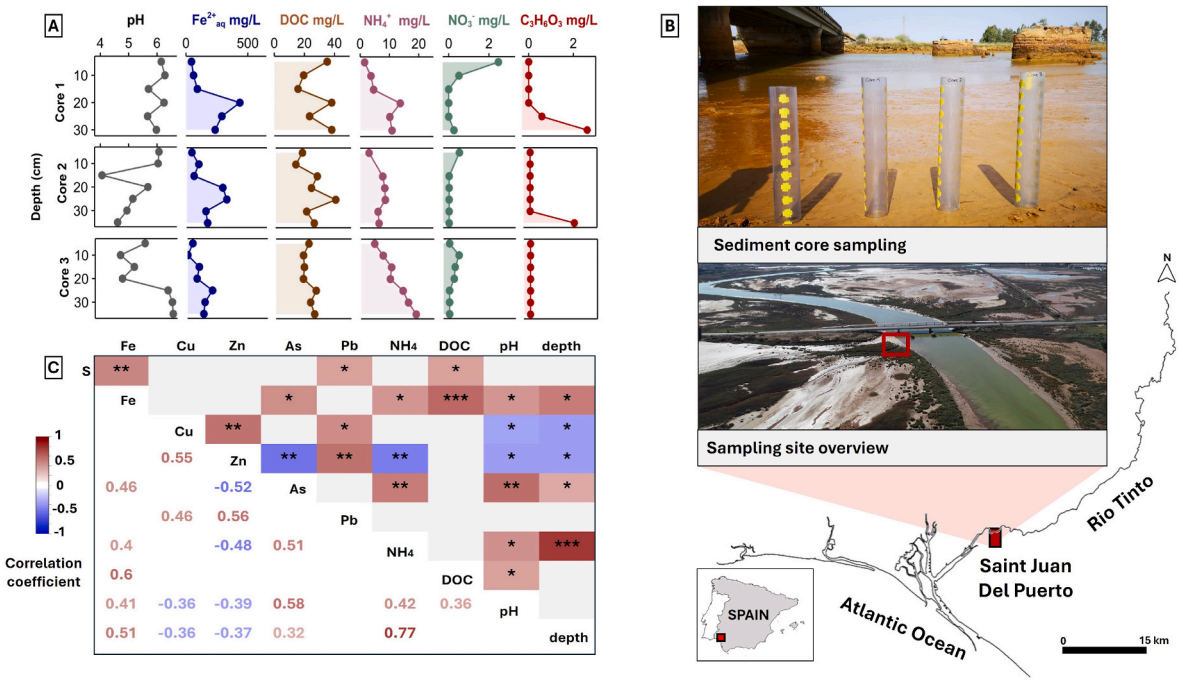

Fig. 2. Sampling site overview and porewater geochemistry of sediment cores collected in the upper estuary of the Río Tinto river near the city of San Juan Del Puerto (A) Porewater geochemical profiles of pH, Fe^{2+}_{aq}, dissolved organic carbon (DOC), NH_4^+, NO_3^- and lactate ($C_3H_6O_3$) over sediment depth of three representative cores indicated as cores 1, 2 and 3. **(B)** Graphical cartography of the Río Tinto basin with the selected coring site in the upper estuary of the river (red square) with its areal overview (sampling overview) and close-up on the actual cores sampling spot (sediment core sampling). **(C)** Correlation analysis between different porewater geochemical parameters, $p < 0.0001$ (***), $p < 0.001$(**) and $p < 0.05$ (*). Correlation coefficients that were not significant were not included (grey boxes). (For interpretation of the references to color in this figure legend, the reader is referred to the Web version of this article.)

and is due to the different geochemical behavior of the HMs. Since As tends to sorb to Fe(III) minerals it can subsequently be released due to mineral dissolution (at acidic pH) or during Fe(III) mineral reduction and dissolution (Al-Abed et al., 2007; Glodowska et al., 2020). This would therefore explain the positive correlation between As and Fe^{2+}_{aq}. In contrast, Cu, Zn and Pb tend to precipitate and be immobilized as metal sulfides within the sediment at circumneutral pH (Estay et al., 2021). HM mobilization/immobilization processes in the Río Tinto sediment are further discussed in section 3.4. Overall, Fe^{2+}, DOC, NH_4^+ and HMs concentrations were on average higher in the sediment porewater compared to the river water and pH showed higher fluctuations within the sediment compared to the river water.

Based on the collected porewater data, Fe(III) reduction seemed to play an important role within the deeper sediment layers since Fe^{2+}_{aq} (up to 0.5 g/L) was the most abundant element after S (up to 2 g/L) and the major cations and anions. Fe(III)-reducing microorganisms, active in the deeper anoxic sediment layers, are probably responsible for the increase of pH (Jimenez-Castaneda et al., 2020) and simultaneous release of organic carbon (OC) trapped and co-sorbed to the Fe(III) minerals (Patzner et al., 2020; Peiffer et al., 1999). This would explain the concomitant increase of Fe^{2+} and DOC with depth which were up to 100 times and 4 times higher in the porewater compared to river water concentrations, respectively. Sulfate-reducing microorganisms, which are abundant in the Río Tinto sediments (Sánchez-Andrea et al., 2012), can also increase the porewater pH (Yuan et al., 2015). The increase of ammonia with sediment depth is generally related to dissimilatory nitrate reduction to ammonium (DNRA) (Giles et al., 2012). This could explain the 20-fold increase of ammonium within the deeper layers compared to the river water, indicating ongoing N cycling within the sediment.

Despite the low NO_3^- concentration and its detection in only a few porewater samples, this does not rule out the possibility that NRFeOx microorganisms could be active within the sediment. It has been shown that concentrations of NO_3^- can vary seasonally, reaching up to 29 mg/L during the spring months (Abramov et al., 2021). Therefore, NO_3^- as an electron acceptor could be constantly supplied by the river due to agricultural activities or could potentially be produced within the sediment by nitrifying microorganisms (Mortimer et al., 2004) while Fe^{2+}, as an electron donor, can be produced within the sediment by Fe (III) reduction. The NO_3^- can undergo a rapid turnover within the sediment under anoxic conditions (Bowles and Joye, 2011; Pan et al., 2022), especially when present in lower concentrations. It could be therefore possible that "cryptic Fe cycling" occurs within the Río Tinto sediment due to the simultaneous activity of Fe(III)-reducing, sulfate-reducing and NRFeOx microorganisms ((Kappler and Bryce, 2017; Peng et al., 2019; Reyes et al., 2016). In order to understand which microorganisms could perform NRFeOx processes within the estuarine sediment of the Río Tinto, we examined the *in-situ* microbial community at different sediment depths.

3.3. *In-situ microbial community composition and potential activity of the estuarian sediment*

Abundances of specific phyla or genera are expressed as DNA-based relative 16S rRNA gene abundances (shortened to % DNA-based in the text) while RNA-based relative 16S rRNA gene abundances (shortened to % RNA-based in the text) indicate their potential activity. RNA extractions from sediments collected at 5 and 10 cm depth were not successful, therefore, conclusions on RNA-based data are only drawn from samples collected at 15, 20, 25 and 30 cm depth. The bacterial community data described in this chapter refer to sediment samples collected from core 1 at different depths (the corresponding mineralogical and geochemical characteristics of this specific core were already described in sections 3.1 and 3.2, respectively). We found that within the first top 15 cm of the core, the Proteobacteria were the most abundant phylum (32.55 ± 1.38 % at 5 cm, 16.54 ± 0.23 % at 10 cm and 27.27 ± 2.36 % at 15 cm depth) (Fig. 3A). RNA analysis indicated that they were especially active at 15 cm depth (30.49 ± 4.55 %) (Fig. S6A). In the deeper layers, the

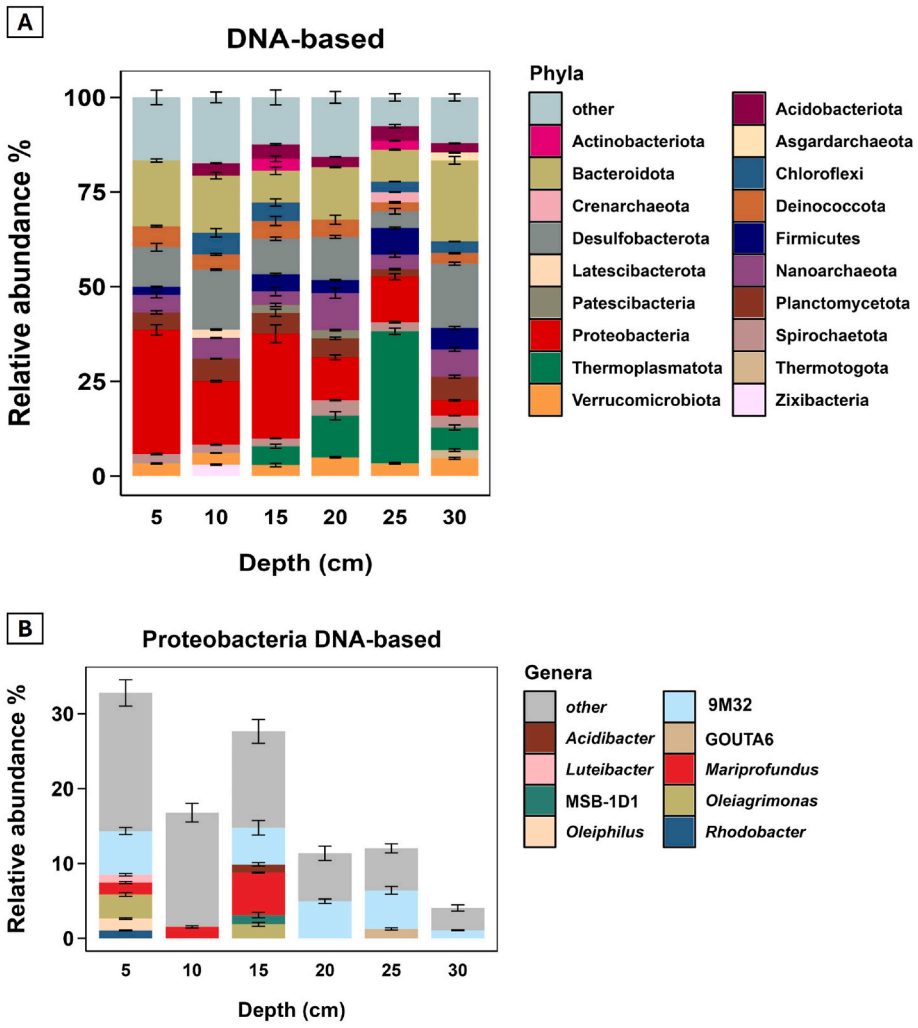

Fig. 3. Microbial community of sediment core 1 (A) DNA-based relative 16S rRNA gene relative abundances of the main phyla at different depth of core 1. **(B)** DNA-based relative 16S rRNA gene relative abundances of the main Proteobacteria genera at different depth of core 1. Phyla and genera with relative abundances lower than 1 % are shown as "other" in the graphs.

Proteobacteria decreased both in terms of relative abundance (11.24 ± 0.60 % at 20 cm, 11.99 ± 0.78 % at 25 cm and 4.02 ± 0.15 % at 30 cm depths; DNA-based) and potential activity (10.49 ± 0.98 % at 20 cm, 9.18 ± 0.53 % at 25 cm and 3.48 ± 0.35 % at 30 cm; RNA-based) while the Desulfobacterota and the Bacteroidota overall became the most abundant phyla. The Desulfobacterota members, known to be involved in sulfur cycling (Sun et al., 2023), were shown to be abundant (up to 15.78 ± 0.19 % at 10 cm and 16.95 ± 0.40 % at 30 cm depths; DNA-based) and potentially active (RNA-based) in all the investigated sediment layers and especially at 30 cm depth (27.47 ± 0.64 %). Abundances of the Bacteroidota phylum were above 14 % (DNA-based) at 5, 10, 20, 30 cm depths but decreased to 8 % at 15 and 25 cm depth, which were the depths characterized by a lower pH (pH 5.7 at both depths, see section 3.1). The potential activity (RNA-based) of the Bacteroidota phylum overall increased over depth (from 4.67 ± 1.41 % at 15 cm depth to 18.64 ± 0.90 % at 30 cm depth) possibly indicating increased importance of fermentation processes in the deeper part of the sediment (Tang et al., 2010). Members of the Firmicutes phylum, typically involved in fermentation (Huang et al., 2023) and Fe(III) reduction (Dong et al., 2020) processes, were also of higher relative abundance at higher depths (from 2.1 ± 0.14 % at 15 cm depth to 7.08 ± 0.25 % at 25 cm depth DNA-based) but their potential activity (between 2.5 and 4 %) did not significantly increase over depth. The members of the Actinobacteriota phylum, also known to be involved in Fe(III) reduction (L. Zhang et al., 2019), were detected and probably active only at 15 and 25 cm depth (DNA-based: 3.21 ± 0.74 % and 2.33 ± 0.06 %; RNA-based: 2.38 ± 0.46 % and 2.81 ± 0.27 %). Such Fe(III)-reducing microorganisms could be favoured by the acidic conditions and abundance of poorly-crystalline Fe(III) minerals (Küsel et al., 1999).

Since most of the existing Fe(II)-oxidizing microorganisms (Hedrich et al., 2011), N-cycling microorganisms (Isobe and Ohte, 2014; Li et al., 2023) and NRFeOx isolates and enrichment cultures are members of the Proteobacteria (Straub et al., 2004; Kappler et al., 2005; Huang et al., 2022b), we described this phylum further at the genus level (Fig. 3B, DNA-based and Fig. S6B, RNA-based). *Mariprofundus*, a known halotolerant microaerophilic Fe(II)-oxidizing microorganism (K. Laufer et al., 2017), was the most abundant (5.67 ± 0.05 %) and potentially active (9.40 ± 0.88 %) genus at 15 cm depth. Less abundant and potentially active microaerophiles such as *Marinobacter* (up to 0.87 ± 0.08 % DNA-based 5 cm depth) and *Acidihalobacter* (up to 0.08 ± 0.001 % DNA-based; 5 cm depth) were also present (Khaleque et al., 2020; Jain et al., 2021). *Mariprofundus*, *Marinobacter* and *Acidihalobacter* were also previously detected in the estuarine sediment and water column of the Río Tinto (Abramov et al., 2021).

Known NRFeOx microorganisms such as *Thiobacillus* (detected only at 20 and 30 cm depth, respectively, with 0.10 ± 0.01 % and 0.09 ± 0.01 %; DNA-based) and *Pseudomonas* (detected only at 20 cm depth with 0.20 ± 0.20 %; RNA-based) were present in the deeper sediment

layers, while *Rhodanobacter* (detected at 5 cm depth with 0.082 ± 0.01 %; DNA-based) was present and potentially active within the surface sediment (Das et al., 1998; Schalk and Perraud, 2023; Hao et al., 2024). Moreover, the genus *Marinobacter* was previously shown to be also potentially capable of NRFeOx (Huang et al., 2022a). Our data also indicated that the genus 9M32 was the most relative abundant (up to 5.1 ± 0.51 % DNA-based) and probably active (up to 4.5 ± 0.44 % RNA-based at 25 cm depth) at different depths (Fig. 3). This genus belongs to the *Acidithiobacillaceae* family, which hosts bacteria involved in N and Fe cycling (Moya-Beltrán et al., 2021) as chemolithoautotrophic acidophilic bacteria are able to oxidize Fe(II) (Kelly and Wood, 2000). Hence, members of this genus may also contribute to Fe(II) oxidation (Boase et al., 2024) in the Río Tinto sediments. Other genera of the Proteobacteria phylum present within the sediments and known to be involved in Fe cycling processes, specifically Fe(III) reduction, were *Rhodobacter* (up to 1.05 ± 0.08 % DNA-based at 5 cm depth) (Dobbin et al., 1996), *Acidibacter* (up to 1.1 ± 0.22 % DNA-based at 15 cm depth) (Falagán and Johnson, 2014) and *Acidiphilium* (up to 0.41 ± 0.01 % DNA-based at 15 cm depth) (Küsel et al., 1999). Some members of the genus *Rhodobacter* are also capable of phototrophic Fe(II) oxidation (Poulain and Newman, 2009), potentially explaining why their relative abundance was higher in the top layer (5 cm depth).

Overall, we observed that in the "reddish-oxidized sediment", microaerophilic and phototrophic Fe(II)-oxidizers (such as *Mariprofundus* and *Rhodobacter,* respectively) are the main microorganisms involved in Fe(II) oxidation especially when oxic/microoxic conditions are established during low tide (when the sediment core was sampled). The establishment of anoxic conditions during high tide could induce a shift in the sediment mineralogy (formation of "black-reduced layer") and microbial community favouring fermenting microorganisms Fe(III) reducers, sulfate reducers and NRFeOx microorganisms such as *Rhodanobacter*, *Thiobacillus* and *Pseudomonas*. Therefore, to target specific NRFeOx microorganisms tha are active in the "reddish-oxidized sediment" under fully anoxic conditions (that could be induced during high tide), laboratory incubation experiments (microcosm experiments) were performed.

3.4. Evaluation of Fe(II) oxidation coupled to nitrate reduction in microcosm experiments –geochemistry

To investigate the activity of NRFeOx favoured by the establishment of anoxic conditions in the sediment during high tide, the "reddish-oxic" sediment was mixed with anoxic medium to achieve brackish water conditions with a slightly acidic pH of 6, simulating the influx of saline water and the increase in pH (as discussed in the introduction). The elemental composition of the final liquid phase in the sediment microcosms is shown in Table S3. Different combinations of Fe^{2+}_{aq} (as electron donor), NO_3^- (as electron acceptor) and C sources (lactate or acetate) were added to each setup and re-spiked when fully consumed for a total of 3–4 times. A biotic control (no amendments) and an abiotic control (addition of NaN_3) were followed over time and compared with the other setups.

One set of microcosms was amended with lactate only (2 mM added in total) since lactate was detected *in-situ* in few porewater samples (Fig. 2A cores 1 and 2, Fig. S5 core 4). In this lactate-amended setup, some acetate was produced (up to 0.3 mM) after full lactate consumption, and Fe^{2+}_{aq} increased up to 11.4 ± 0.8 mM within 44 days of anoxic incubation (Fig. 4A). The rate of Fe^{2+}_{aq} release was almost 4 times higher (0.26 mM Fe^{2+}_{aq}/day) compared to the biotic control (0.07 mM Fe^{2+}_{aq}/day). The pH increase was also higher 42 days after addition of lactate (from 6.0 ± 0.0 to7.0 ± 0.0) compared to the biotic setup (from 6.0 ± 0.0 to 6.2 ± 0.0, Fig. S7A) and abiotic setup (from 6.0 ± 0.0 to 6.0 ±

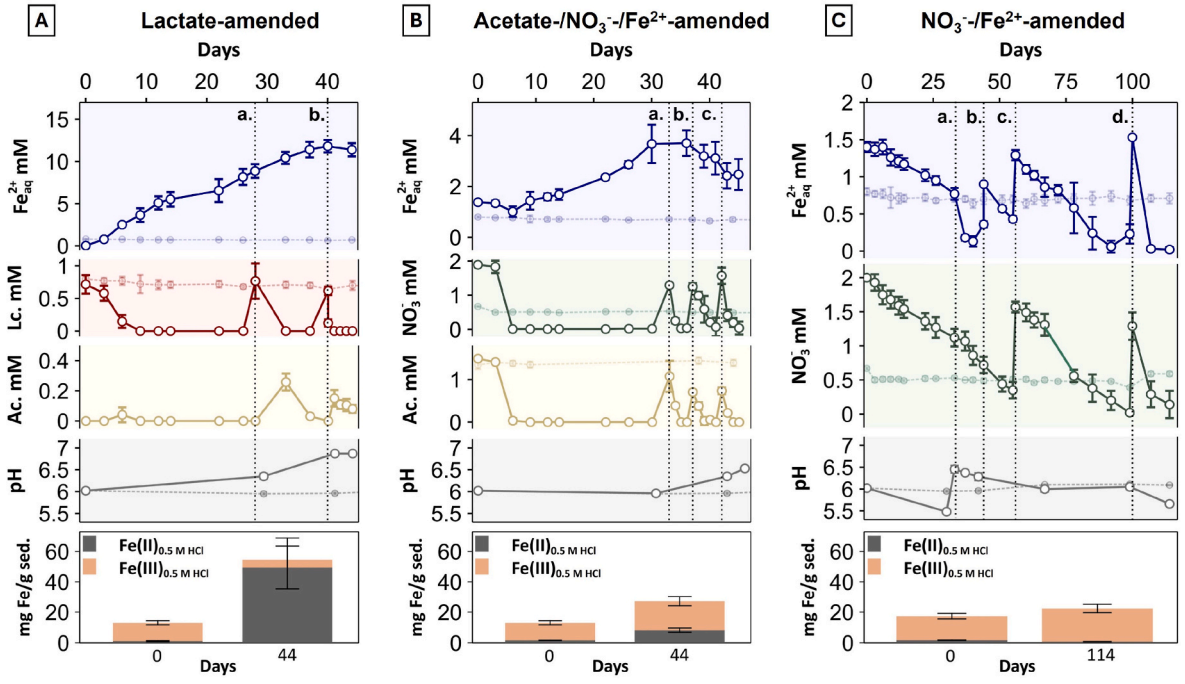

Fig. 4. Geochemistry and minerology of microcosm experiments (A) Changes in Fe^{2+}_{aq} (in blue), lactate (in red), acetate (in yellow) and pH (in grey) over 44 days in the microcosm setup amended only with lactate. The dashed lines a. and b. indicate the re-addition of lactate. **(B)** Changes in NO_3^- (in green), Fe^{2+}_{aq} (in blue) and acetate (in yellow) concentrations and pH over 44 days in the acetate-/NO_3^-/Fe^{2+}-amended microcosm. The dashed lines a., b. and c. indicate the re-addition of acetate and NO_3^-. **(C)** Changes in NO_3^- (in green) and Fe^{2+}_{aq} (in blue) concentrations and pH in the NO_3^-/Fe^{2+}-amended microcosm over 114 days of incubation. The dashed line a. indicates the time-point of pH adjustment while dashed line b. indicates the time-point of Fe^{2+}_{aq} re-addition. Dashed lines c. and d. indicate re-addition of both Fe^{2+}_{aq} and NO_3^-. The abiotic control (amended with NaN_3) data are shown in lighter colour with dashed lines. Acidic sequential Fe extractions targeting the poorly crystalline Fe phase (0.5 M HCl), performed for each setup at the beginning and end of the experiment, are shown in the bottom part of the respective graph. Orange bars indicate the 0.5 M HCl extractable mg Fe(III)/g of dry sediment while grey bars indicate the 0.5 M HCl extractable mg Fe(II)/g of dry sediment. (For interpretation of the references to color in this figure legend, the reader is referred to the Web version of this article.)

0.0). Furthermore, almost complete transformation of poorly crystalline (bioavailable) Fe(III) minerals into poorly crystalline Fe(II) minerals (increase of Fe(II) minerals from 1.0 ± 0.3 to 49.5 ± 14.0 mg Fe(II)/g dry sediment) was observed within 44 days. By using 0.5 M HCl both sorbed Fe(II) and poorly crystalline Fe(II) mineral phases can be targeted (Fredrickson et al., 1998), therefore, the amount of extracted Fe(II) with 0.5 M HCl will be referred as solid-associated Fe(II) in the text. However, a clear mineralogical transformation was also observed visually since the originally reddish sediment turned completely black (Picture S3).

Altogether, the increase of pH, Fe^{2+}_{aq}, solid-associated Fe(II), as well as the transformation of lactate to acetate, strongly suggested that Fe(III) reduction took place during anoxic incubation in the lactate-amended setup (O'loughlin et al., 2021). Since the production of acetate, increase of pH, Fe^{2+}_{aq} and increase of solid-associated Fe(II) were not observed in the abiotic setup (Fig. S7C), Fe(III) reduction was most likely a biotic process catalyzed by sulfate-reducing and Fe(III)-reducing microorganisms. Assuming that all lactate (2 mM) was converted to acetate during Fe(III) reduction (releasing 4 electrons), the theoretical amount of the released Fe^{2+}_{aq} should correspond to 8 mM at the end of the experiment. However, this value is lower than what we measured at the end of the incubation period (11.4 mM Fe^{2+}_{aq}). This difference could be due to the activity of Fe(III)-reducing microorganisms, which can also use the produced acetate as electron donor (Finneran et al., 2003; Tor et al., 2001) or from the oxidation of additional organic carbon mobilized during Fe(III) mineral reduction. Indeed, the setup amended with lactate showed the highest increase of DOC (from 17.8 ± 7.2 mg/L to 54.1 ± 3.8 mg/L) (Fig. S8). This could result from fermentation processes of particulate organic matter (Zhu et al., 2020) or from the release of OC previously bound to Fe(III) minerals during biotic/abiotic Fe(III) reduction and Fe(III) mineral dissolution (Patzner et al., 2020). SRB can also convert lactate to acetate (Luptáková et al., 2015) and be involved in Fe(III) reduction abiotically via sulfide-mediated Fe(III) mineral dissolution ()M.dos and Stumm, 1992. Fermentation, SRB and Fe(III) reduction are generally co-occurring processes (Lentini et al., 2012) since the fatty acids produced during fermentation could be directly used by Fe(III)-reducing and sulfate-reducing microorganisms (Lovley, 1987). In the biotic setup without amendments (biotic control), the same geochemical trends (increase of pH, Fe^{2+}_{aq}, DOC and solid-associated Fe (II)) were observed but to a lesser extent (Fig. S7A,B and Fig. S8).

An additional setup was amended with acetate, NO_3^- and Fe^{2+}_{aq} to target NRFeOx microorganisms favoured by the influx of NO_3^- (as electron acceptor supplied by the river), by the release of Fe^{2+}_{aq} from Fe (III) reduction (as electron donor) and the presence of acetate (as carbon source). In this setup, we observed that both acetate and nitrate were fully consumed within a week. Nitrate reduction rates were 0.31, 0.43, 0.25 and 0.52 mM NO_3^-/day during the first, second, third and fourth amendments, respectively. The consumption of acetate and nitrate coincided with an initial (within the first 7 days) slight decrease of aqueous Fe^{2+}_{aq} during the first, third and fourth amendment (consumption of 0.38 ± 0.21, 0.44 ± 0.45 and 0.62 ± 0.18 mM Fe^{2+}_{aq}, respectively) (Fig. 4B). However, when acetate and nitrate were fully consumed, from day 7 to day 30, the Fe^{2+}_{aq} concentration increased from 1.01 ± 0.21 to 3.6 ± 0.7 mM (0.11 mM Fe^{2+}_{aq}/day). This rate was approximately two times higher than the one calculated for the non-amended biotic microcosm during the same time (0.07 mM Fe^{2+}_{aq}/day) but almost 2 times lower than the rate calculated for the lactate-amended setup. In the acetate-/NO_3^--/Fe^{2+}-amended setup, the solid-associated Fe(II) pool (extractable with 0.5 M HCl) showed a higher increase compared to the biotic control (from 1.6 ± 0.1 to 8.2 ± 1.4 for the acetate-/NO_3^-/Fe^{2+}-amended setup and from 1.1 ± 0.3 to 3.5 ± 0.3 mg Fe(II)/g of dry sediment for the biotic control within 44 days). In the acetate-/NO_3^--/Fe^{2+}-amended setup, the pH and DOC increased over time from 6.0 ± 0.03 to 6.5 ± 0.0 and from 12.3 ± 2.1 to 38.8 ± 1.6 mg/L, respectively. Altogether, the increase of pH, DOC, solid-associated Fe(II) and Fe^{2+}_{aq} in the acetate-/NO_3^-/Fe^{2+}-amended setup (after nitrate consumption), also observed in the biotic control and in the lactate-amended setup, were most likely the result of biotic Fe(III) reduction fuelled by the addition of acetate as previously discussed.

Despite the overall pH increase, the final value in the acetate-/NO_3^--/Fe^{2+}-amended setup was ~0.2 units lower (pH of 6.53 ± 0.04 after 44 days) than in the biotic control (pH of 6.69 ± 0.01 after 44 days). This could be an indication that NRFeOx, a known acidifying process (K. L. Straub et al., 1996), could have been taking place. It has been shown that the presence of NO_3^- and NO_2^- can decrease Fe(III) reduction rates (DiChristina, 1992; S. H. Zhang et al., 2009) and therefore favouring NRFeOx processes (Laufer et al., 2016b). This explains the concomitant decrease of Fe^{2+}_{aq}, nitrate and acetate. During NO_3^- consumption, NO_2^- was produced (up to 0.1 mM) and then subsequently consumed (Fig. S9). A similar appearance and disappearance of nitrite was reported by several studies on NRFeOx enrichment cultures (Bayer et al., 2023; Jakus et al., 2021). The NO_2^- formed initially can be further consumed during denitrification processes or by reacting with Fe(II) in an abiotic process known as chemodenitrification (Klueglein and Kappler, 2013). Chemodenitrification may have a stronger contribution to Fe(II) oxidation in salt water environment, especially in the presence of acetate (Huang et al., 2022a). Due to the fact that organic compounds such as acetate can also stimulate different microbial processes such as Fe(III) reduction and heterotrophic denitrification (Fu et al., 2022), it was not possible to determine whether NRFeOx unambiguously occurred based solely on this geochemical data.

In addition to the microcosms amended with acetate, Fe^{2+}_{aq} and NO_3^-, we also prepared setups with NO_3^- and Fe^{2+}_{aq} (no acetate) to target microorganisms able to reduce NO_3^- and oxidize Fe^{2+} under lower OC conditions. In this setup, nitrate consumption rates were initially 10 times lower (0.03 mM NO_3^-/day in the first and second amendments) than the rates obtained for the acetate-/NO_3^-/Fe^{2+} setup (Fig. 4C). However, after the third amendment, nitrate reduction rates in the NO_3^-/Fe^{2+} were three times higher (0.09 mM NO_3^-/day) compared to the initial rates. NO_2^- was not detected at any time point. Furthermore, the NO_3^--/Fe^{2+}-amended setup was the only microcosm in which a decrease of pH was observed over time. The pH decreased from 6.0 ± 0.0 to 5.4 ± 0.0 during the first amendment and was subsequently re-adjusted to 6.5 ± 0.1 to match the pH values of the other setups and initial conditions (Fig. 4C). The pH kept decreasing during the incubation, reaching a value of 5.7 ± 0.0 at the end of the experiment (114 days).

Following the stoichiometric equation that couples nitrate reduction to Fe(II) oxidation proposed by Straub et al. (1996), the activity of autotrophic NRFeOx microorganisms favours the production of H^+ and therefore acidification. Further evidence for NRFeOx in the NO_3^--/Fe^{2+}-amended setup was the increase of 5.95 ± 0.91 mg Fe(III)/g dry sediment in bioavailable Fe(III) minerals (extractable with 0.5 M HCl). This value was consistent with the theoretical value (5.76 mg Fe (III)/g dry sediment) calculated based on the total amount of Fe^{2+}_{aq} added throughout the experiment, assuming complete oxidation. This confirmed that all the Fe^{2+}_{aq} added was completely oxidized to poorly crystalline Fe(III) minerals which was previously observed in other NRFeOx enrichment cultures (Jakus et al., 2021; Pantke et al., 2012). DOC fluctuated during the experiment (Fig. S8) but overall did not change significantly within the 114 days of incubation (from 8.7 ± 0.7 at the beginning of the experiment to 7.7 ± 1.0 mg/L at the end). The decrease of DOC (especially after re-addition of Fe^{2+}, Fig. 4C time-points a, b, c and d) could be linked to the formation OC-Fe(III) aggregates (sorption of OC to and co-precipitation of OC with Fe(III) minerals) which usually occurs during and after Fe(II) oxidation. The presence of OC-Fe(III) minerals was also observed within the *in-situ* sediment (Fig. 1D). The increase of DOC and Fe^{2+}_{aq} observed after full NO_3^- consumption (and before the next Fe^{2+} and NO_3^- re-addition) suggests the occurrence of Fe(III) reduction.

Since our geochemical data strongly suggested the presence of NRFeOx in the NO_3^--/Fe^{2+}-amended microcosm, $NO_{3\,reduced}^-$:$Fe(II)_{oxidized}$ ratios could be calculated and compared to the theoretical value of 0.2 assuming autotrophic NRFeOx and formation of N_2 as the end product

(not considering the electrons from Fe(II) oxidation needed for CO_2 reduction). After each amendment period, the calculated $NO_{3\,reduced}^{-}$:$Fe(II)_{oxidized}$ ratios were higher than the theoretical value (1.70 during the first, 1.46 during the second and 0.76 during the third amendment, respectively) meaning that more NO_3^- was reduced than Fe(II) oxidized. This indicates that other processes such as heterotrophic denitrification or mixotrophic NRFeOx occurred (Laufer et al., 2016a,b). It has to be noted that simultaneously occurring Fe(III) reduction could also impact these calculations. Another type of microorganism that could compete with NRFeOx are dissimilatory nitrate reduction to ammonium (DNRA) microorganisms (Tiedje, 1988). In environments both rich in organic carbon and nitrate, DNRA microorganisms may outcompete other denitrifies such as NRFeOx microbes for nitrate (van den Berg et al., 2016). Therefore, the presence of DNRA microorganisms, together with heterotrophic denitrifying microorganisms, could result in an overestimation of NRFeOx contribution.

In conclusion, our microcosm experiments data suggested that Fe(III) reduction was the main processes occurring when the oxidized sediment was made anoxic (without nitrate being present as electron acceptor), especially, when readily metabolizable OC compounds produced by fermenters (such as lactate or acetate) were present. The release of Fe_{aq}^{2+} and OC during Fe(III) mineral reduction, the increase of pH and the conversion of lactate to acetate could favour mixotrophic NRFeOx microorganisms when NO_3^- is transported from the river to the sediment. Meanwhile, autotrophic NRFeOx microorganisms thriving under low OC conditions (when NO_3^- is present) can induce geochemical changes such as porewater acidification and production of poorly crystalline Fe(III) minerals. To provide clear evidence of ongoing NRFeOx we analyzed the microbial composition and activity of our microcosms.

3.5. Evaluation of Fe(II) oxidation coupled to nitrate reduction in microcosm experiments –microbial community

Sediment sampling for DNA and RNA extraction at the beginning of the experiment (referred to as "initial" in Fig. 5) was conducted on three additional bottles that were set up simultaneously and identically to the other setups (as described in section 2.3) but without any amendment. Sediment sampling for DNA and RNA extraction from the actual setups and controls was conducted only at the end of the experiment, with timing varying depending on the specific setup. The non-amended setup (-biotic control), the NaN_3-amended setup (abiotic control) and the NO_3^--/Fe^{2+}-amended setups were sampled after 114 days while the lactate-only and acetate-/NO_3^--/Fe^{2+}-amended setups were sampled after 44 days since the substrates were consumed faster.

The initial bacterial community was dominated by Proteobacteria (49.9 ± 0.5 % DNA-based and 48 ± 2 % RNA-based) (Fig. 5A and B). Within this phylum, the most abundant genera involved in Fe cycling were: Fe(III)-reducers such as *Acidibacter* (1.4±% DNA-based and 1.76 ± 0.06 % RNA-based) and *Acidiphilium* (0.5 % and 0.88 ± 0.08 % RNA-based), phototropic Fe(II)-oxidizers such as *Rhodobacter* (0.96 ± 0.5 % DNA-based and 3.26 ± 0.64 % RNA-based), microaerophilic Fe(II)-oxidizers such as *Mariprofundus* (1.09 ± 0.55 % DNA-based and 1.79 ± 0.05 % RNA-based) and *Marinobacter* (0.92 ± 0.11 % DNA-based and 1.93 ± 0.06 % RNA-based) and potential NRFeOx microorganisms such

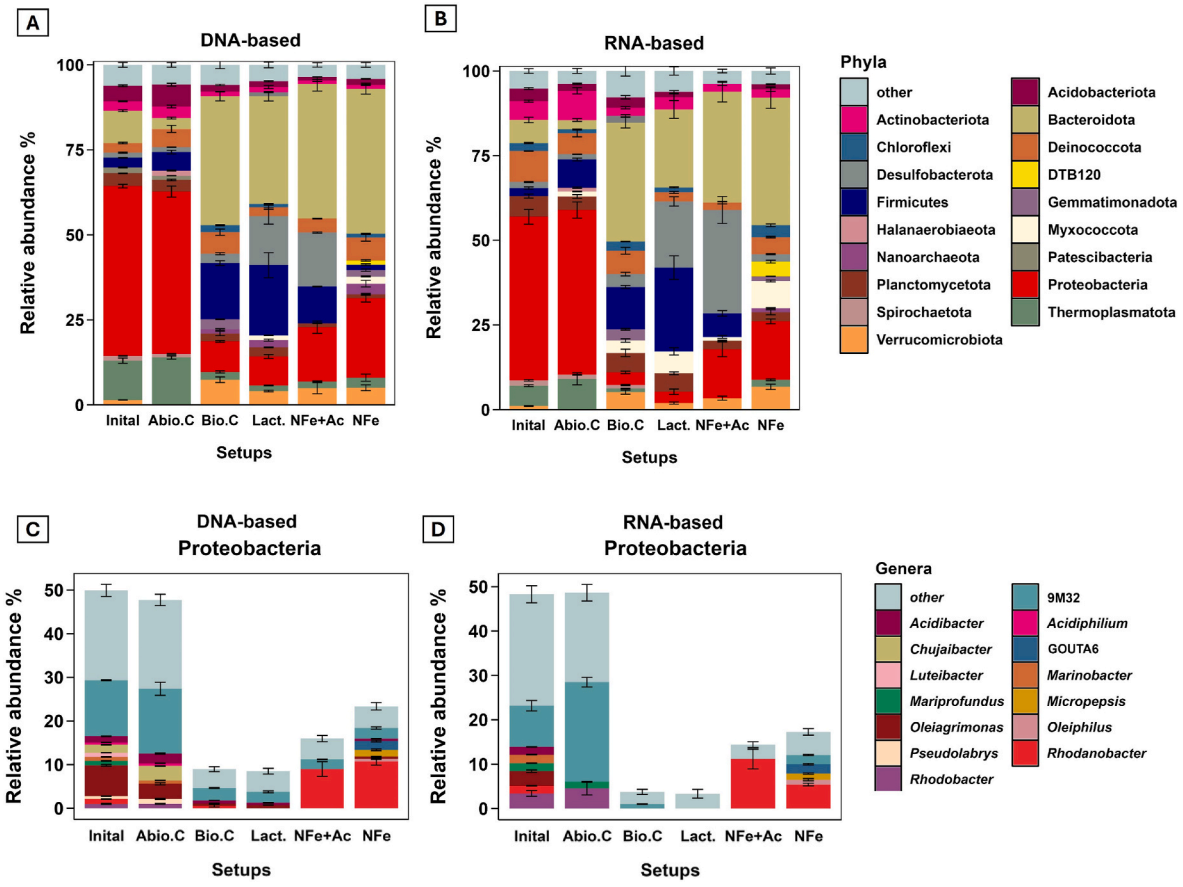

Fig. 5. Microbial community of microcosm experiments (A) DNA-based and **(B)** RNA-based 16S rRNA gene relative abundances of selected phyla in the different setups/controls. **(C)** and **(D)** refer to DNA-based and RNA-based 16S rRNA gene relative abundances of the Proteobacteria phylum at a genus level. Samples for sequencing were taken at different time points: day 0 (initial), day 44 (Lactate and NFe + Ac setup) and day 114 (abiotic, biotic controls and NFe setup). Phyla and genera with relative abundances lower than 1 % are shown as "other" in the graphs. NFe + Ac refers to the acetate-/NO_3^--/Fe^{2+}-amended setup while NFe refers to the NO_3^--/Fe^{2+}-amended setup.

as *Rhodanobacter* (1.12 ± 0.21 % DNA-based and 1.71 ± 0.08 % RNA-based) (Fig. 5B and C). These genera were also present in the *in-situ* bacterial community of the "oxic layer sediment" (chapter 3.3). Overall, the microbial community of the sediment used for the microcosm experiment was not significantly different from the *in-situ* microbial community of core 1 (Fig. S10 A and C). The microbial community of the abiotic control and lactate-amended setups did not show any significant changes after 114 days and 44 days of incubation respectively compared to the initial conditions.

The setups with NO_3^- addition (acetate-/NO_3^--/Fe^{2+}- and/NO_3^--/Fe^{2+}-amended setups) were shown to be significantly different from the initial conditions (Fig. S10 B and D). Specifically, the Proteobacteria decreased over time in all the setups, except for the abiotic control, while the Bacteroidota became the most abundant phylum (up to 42.08 ± 0.21 % DNA-based and 37.7 ± 3.1 % RNA-based in the NO_3^--/Fe^{2+}-amended setup after 114 days). Additionally, when Fe(III) reduction was observed (biotic control, lactate-only and acetate-/NO_3^--/Fe^{2+}-amended setups; section 3.3), the abundance and potential activity of the Firmicutes (with the highest increase in the lactate-amended setup) and Desulfobacterota phyla increased over time (especially in the acetate-/NO_3^--/Fe^{2+}-amended setup). The decrease of Proteobacteria and concomitant increase of the Bacteroidota, Desulfobacterota and Firmicutes phyla (both in terms of abundances and potential activities) was also observed in the deeper sediment layers of core 1 (a described in section 3.2). The overall shift in the bacterial community, compared to the initial conditions, was most likely induced by the establishment of anoxia during the incubation period. In fact, the activity of fermenting microorganisms belonging to the phyla Firmicutes and Bacteroidota is generally favoured under anoxic conditions (Huang et al., 2023). More specifically, *Lutibacter* was the main fermenting microorganism (Wissuwa et al., 2017) enriched in the biotic, NO_3^-/Fe^{2+}-amended setup and acetate-/NO_3^--/Fe^{2+}-amended setup, while *Ignavibacterium* was the most abundant fermenter (Bei et al., 2021) in the lactate-amended setup and in the biotic control (Fig. S11A.). The addition of C sources (in the only lactate- and acetate-/NO_3^--/Fe^{2+}-amended setups) increased the abundance and activity of the Desulfobacterota phylum. Such microorganisms are known to perform dissimilatory sulfate reduction under anoxic conditions (Diao et al., 2023) facilitating Fe(III) mineral reduction processes within the sediments (Coleman et al., 1993). *Geotalea* (Fig. S11B.) was the most abundant genus belonging to the Desulfobacterota enriched in the acetate-/NO_3^--/Fe^{2+}-amended setup. Considering the similarities between the genus *Geotalea* and *Geobacter*, these microorganisms could be mainly responsible for Fe(III) reduction processes (Xie et al., 2023). Additionally, Fe(III) reduction in the lactate-amended setup could be potentially carried by both the genera *Geotalea* and *Clostridium* (Wang et al., 2023). Overall, the increased activity of Fe(III)-reducing microorganisms (such as the *Geotalea* and the *Clostridium* genera) explained the increase of Fe^{2+}_{aq}, Fe(II) minerals and pH observed in the setups with addition of acetate and lactate. Additionally, the increased activity of fermenting microorganisms as the *Lutibacter* and the *Ignavibacterium* genera (also observed in the biotic setup) justified the increase of DOC values observed in the biotic control, only lactate- and acetate-/NO_3^--/Fe^{2+}-amended setups. Similar geochemical trends (such as the increase of pH, Fe(II) minerals, Fe^{2+}_{aq}, DOC as described in chapter 3.2) and microbial community composition changes (such as the decrease of Proteobacteria and concomitant increase of the Bacteroidota, Desulfobacterota and Firmicutes phyla observed in the sediment core 1, described in section 3.3) were also observed in the deeper "reduced black sediment layers" of the Río Tinto sediment.

In contrast, in the setup with the addition of nitrate (NO_3^--/Fe^{2+}- and acetate-/NO_3^--/Fe^{2+}-amended setups), abundances and potential activities of the Proteobacteria (23.36 ± 1.23 % DNA-based and 17.26 ± 0.71 % RNA-based for the NO_3^--/Fe^{2+}-amended setup; 15.97 ± 1.82 % DNA-based and 14.42 ± 2.17 % RNA-based for the acetate-/NO_3^--/Fe^{2+}-amended setup) phylum were higher than the setups without NO_3^- addition. Specifically, when nitrate was added, the genus *Rhodanobacter* became the most abundant genus within the Proteobacteria phylum, increasing from 1.12 ± 0.05 % (DNA-based) to 8.99 ± 1.66 % (DNA-based) in the acetate-/NO_3^--/Fe^{2+}-amended setup and to 10.75 ± 0.88 % (DNA-based) in the NO_3^--/Fe^{2+}-amended setup after 44 and 114 days of incubation respectively. Members of the *Rhodanobacter* genus, which were already present in the upper layer (5 cm) of core 1 (as discussed in section 3.3), were reported to thrive both in acidic and circumneutral nitrate-rich conditions and described as slow-growing microorganisms capable of full denitrification (Green et al., 2012). Additionally, metagenomic analysis of the NRFeOx enrichment culture KS highlighted that *Rhodanobacter* possess transcript and proteins involved in Fe(II) oxidation and denitrification. However, in this specific enrichment culture, Fe (II) oxidation is carried out by *Gallionella* while *Rhodanobacter* completes denitrification (Huang et al., 2021). Nonetheless, *Rhodanobacter* could also be capable of carrying NRFeOx in different bacterial consortia as recently shown by Hao et al. (2024). In that study, the addition of Fe(II) source stimulated the expression of denitrification genes and upregulation of the *feoB* gene facilitating the entry of Fe(II) into the periplasm for reaction with NOx-N carried out by *Rhodanobacter*. The potential activity of *Rhodanobacter* was higher in the setup amended with acetate compared to the one without (11.15 ± 2.24 % and 5.40 ± 0.30 % RNA-based in the acetate-/NO_3^--/Fe^{2+}-amended setup and NO_3^--/Fe^{2+}-amended setup, respectively). The higher potential activity of *Rhodanobacter* could be due to the presence of acetate since NRFeOx microorganisms are known to gain more energy and replicate faster under mixotrophic conditions (Muehe et al., 2009). This would therefore explain why nitrate reduction rates were slower without the addition of acetate, as described in the previous section. Moreover, in the acetate/NO_3^-/Fe^{2+}-amended setup, the potential activity (RNA-based) of the genus *Rhodanobacter* was on average higher than its relative abundance (DNA-based) after 44 days of incubation, suggesting that the addition of acetate effectively stimulated both the growth and metabolic activity of this genus. In contrast, in the NO_3^-/Fe^{2+}-amended setup (without acetate), DNA-based relative abundances of *Rhodanobacter* were consistently higher than RNA-based ones. This would further confirm that while *Rhodanobacter* was present, its activity was limited in the absence of an external organic carbon source. Members of the uncharacterized phylum DTB120 (1.22 ± 0.21 % DNA-based and 4.31 ± 0.40 %RNA-based), present only in the NO_3^--/Fe^{2+}-amended setup, were recently shown to also be capable of NRFeOx processes (McAllister et al., 2021). This suggests the potential of finding novel, uncharacterized NRFeOx bacteria which do not belong to the Proteobacteria phylum (as for all the other microorganisms capable of this metabolism) in the estuarian sediment of the Río Tinto. Furthermore, in the NO_3^--/Fe^{2+}-amended setups, members of the Firmicutes and Desufobacterota phyla did not increase in abundance nor activities over time indicating that Fe(III) reduction processes were inhibited in this setup due to the continuous supply of nitrate and low OC concentrations. However, we acknowledge that our data interpretation was solely based on geochemical analysis and 16S rRNA gene abundances while lacking more direct functional genes evidence (e.g. *nir* or *feoB* genes). Future studies integrating metagenomics and transcriptomics analysis will be essential to confirm the NRFeOx capability of *Rhodanobacter* and members of the DTB120 phylum.

In summary, the microbial community changes complemented the observed geochemical trends (section 3.4) in each microcosm experiment confirming that the exposure of the oxidized (orange) sediments to anoxic conditions initially favoured fermentation and Fe(III) reduction. However, the supply of nitrate by the river and by-products of lactate-based Fe(III) reduction (Fe^{2+}_{aq} and acetate), stimulated NRFeOx microorganisms such as *Rhodanobacter* and allowed cryptic Fe cycling within the Río Tinto sediment. NRFeOx microorganisms such as *Rhodanobacter* and potentially also members of the uncharacterized phylum DTB120, could have a higher contribution to Fe cycling within low-OC sediment microinches. Our results further highlight the capability of members of

the *Rhodanobacter* genus to carry out NRFeOx and reveal their adaptability to acidic and high salinity environments.

4. Environmental implications and conclusions

The potential activity of NRFeOx microorganisms within the Río Tinto sediments, as demonstrated in the previous chapters, could favour nitrate pollution attenuation and simultaneously immobilize HMs within the sediment. Considering the elevated concentrations of HMs both in the sediment and in the Río Tinto water, NRFeOx microorganisms could support *in-situ* remediation by biotically producing Fe(III) (oxyhydr)oxides and co-precipitating HMs (Xiu et al., 2019), which are then immobilized within the anoxic sediment. Geochemical data obtained from the microcosm experiments (described in section 3.4) demonstrated that, after 114 days of incubation, the Zn, As and Cr concentrations increased in the biotic control (the overall increase compared to the initial conditions was 16.3 ± 0.1 mg/L for Zn and 50.0 ± 10.0 μg/L for As and 20 ± 10.0 μg/L for Cr, Fig. S12). An even higher increase of Zn and As (the overall increase compared to the initial conditions was 4.7 ± 0.6 mg/L for Zn and 110.0 ± 30.0 μg/L for As) was observed in the lactate-amended setups. In the acetate-/-NO_3^--/Fe^{2+}-amended setups, the increase of As was observed in only one replicate (the increase compared to the initial conditions was of 150 μg/L) after 44 days of incubation. A different trend was observed for the NO_3^--/Fe^{2+}-amended setups since As was not mobilized and Zn increased comparably to the abiotic control during the 114 days of incubation. These results could indicate that when anoxic conditions are established within the sediment and nitrate is not present, Fe(III) reduction could favour As and Zn release from the sediment to the porewater. The production of acetate and lactate by fermenting bacteria can increase the activity of Fe(III)-reducing microorganisms enhancing As and Zn mobilization by biotic reductive Fe(III) mineral dissolution (Kontny et al., 2021). In contrast, the presence of nitrate could stimulate the activity of NRFeOx microorganisms minimizing As and Zn mobilization under anoxic conditions induced by high tidal activity. Considering these results, further efforts on the enrichment and isolation of NRFeOx microorganisms thriving in such an extreme environment, along with assessments of their pH and salinity tolerance, could offer new bioengineering applications for simultaneous removal of NO_3^- and HMs in AMD-like contaminated water bodies.

CRediT authorship contribution statement

Martina Bottaro: Writing – review & editing, Writing – original draft, Visualization, Methodology, Investigation, Formal analysis, Conceptualization. **Sergey Abramov:** Writing – review & editing, Investigation, Conceptualization. **Ricardo Amils:** Writing – review & editing, Supervision, Methodology. **Adrian Martinez-Bonilla:** Writing – review & editing, Methodology, Investigation. **Laurel ThomasArrigo:** Writing – review & editing, Methodology, Formal analysis. **Daniel Straub:** Writing – review & editing, Supervision, Formal analysis. **Muammar Mansor:** Writing – review & editing, Supervision, Methodology, Formal analysis. **Sara Kleindienst:** Writing – review & editing, Supervision, Formal analysis. **Andreas Kappler:** Writing – review & editing, Supervision, Resources, Project administration, Methodology, Funding acquisition, Conceptualization.

Data availability

Research data will be uploaded to the FDAT Repository at the University of Tübingen. Raw sequencing data has been deposited at NCBI in the Sequence Read Archive (SRA) under BioProject accession number PRJNA1183296 (https://www.ncbi.nlm.nih.gov/bioproject/PRJNA1183296).

Declaration of competing interest

The authors declare the following financial interests/personal relationships which may be considered as potential competing interests: Andreas Kappler reports financial support was provided by German Research Foundation (DFG). If there are other authors, they declare that they have no known competing financial interests or personal relationships that could have appeared to influence the work reported in this paper.

Acknowledgments

This work was founded by the German Research foundation. A. K. acknowledges infrastructural support by the DFG under Germany's Excellence Strategy, cluster of Excellence EXC2124, project ID 390838134. We would like to thank the Institute for Medical Microbiology and Hygiene (MGM, where the NGS sequencing methods were performed) of the University of Tübingen with the support of the DFG-funded NGS Competence Centre Tübingen. We also acknowledge the synchrotron radiation facilities ELETTRA (proposal nr. 20225213) and thank Luca Olivi (XAFS beamline) for his help during the data collection. We also thank Cristina Escudero for providing reference materials (Pyrite and Magnetite) for synchrotron analysis. Overall, we would like to thank Lars Grimm for his support during the field campaigns, Franziska Schädler for segmented flow analyzer measurements and DNA/RNA extractions support, Marie Mollenkopf for HPLC measurements, Sören Drabesch for ICP-MS measurements and Tsz Ho Chiu for his help with the microcosm experiments sampling.

Appendix A. Supplementary data

Supplementary data to this article can be found online at https://doi.org/10.1016/j.apgeochem.2025.106488.

Data availability

Data will be made available on request.

References

Abramov, S.M., Tejada, J., Grimm, L., Schädler, F., Bulaev, A., Tomaszewski, E.J., Byrne, J.M., Straub, D., Thorwarth, H., Amils, R., Kleindienst, S., Kappler, A., 2020. Role of biogenic Fe(III) minerals as a sink and carrier of heavy metals in the rio tinto, Spain. Sci. Total Environ. 718. https://doi.org/10.1016/j.scitotenv.2020.137294Afonso.

Abramov, S.M., Straub, D., Tejada, J., Grimm, L., Schädler, F., Bulaev, A., Thorwarth, H., Amils, R., Kappler, A., Kleindienst, S., 2021. Biogeochemical niches of Fe-cycling communities influencing heavy metal transport along the rio tinto, Spain. Appl. Environ. Microbiol. AEM0229021. https://doi.org/10.1128/AEM.02290-21.

Al-Abed, S.R., Jegadeesan, G., Purandare, J., Allen, D., 2007. Arsenic release from iron rich mineral processing waste: influence of pH and redox potential. Chemosphere 66 (4), 775–782. https://doi.org/10.1016/J.CHEMOSPHERE.2006.07.045.

Amils, R., Escudero, C., Oggerin, M., Puente Sánchez, F., Arce Rodríguez, A., Fernández Remolar, D., Rodríguez, N., García Villadangos, M., Sanz, J.L., Briones, C., Sánchez-Román, M., Gómez, F., Leandro, T., Moreno-Paz, M., Prieto-Ballesteros, O., Molina, A., Tornos, F., Sánchez-Andrea, I., Timmis, K., et al., 2023. Coupled C, H, N, S and Fe biogeochemical cycles operating in the Continental deep subsurface of the iberian pyrite belt. Environ. Microbiol. 25 (2), 428–453. https://doi.org/10.1111/1462-2920.16291.

Apprill, A., Mcnally, S., Parsons, R., Weber, L., 2015. Minor revision to V4 region SSU rRNA 806R gene primer greatly increases detection of SAR11 bacterioplankton. Aquat. Microb. Ecol. 75 (2), 129–137. https://doi.org/10.3354/ame01753.

Bayer, T., Tomaszewski, E.J., Bryce, C., Kappler, A., Byrne, J.M., 2023. Continuous cultivation of the lithoautotrophic nitrate-reducing Fe(II)-oxidizing culture KS in a chemostat bioreactor. Environmental Microbiology Reports 15 (4), 324–334. https://doi.org/10.1111/1758-2229.13149.

Bedini, E., Domiciano Galvíncio, J., Chen, J., 2022. Use of NASA's AVIRIS-NG imagery for environmental mapping at the rio tinto mining district, Southwestern Spain. Journal of Hyperspectral Remote Sensing 12 (4), 154–165. https://doi.org/10.29150/JHRS.V12.4.P154-165.

Bei, Q., Peng, J., Liesack, W., 2021. Shedding light on the functional role of the Ignavibacteria in Italian rice field soil: a meta-genomic/transcriptomic analysis. Soil Biol. Biochem. 163. https://doi.org/10.1016/J.SOILBIO.2021.108444.

Boase, K., Santini, T., Watkin, E., 2024. Microbes of biotechnological importance in acidic saline Lakes in the yilgarn craton, Western Australia. Front. Microbiol. 15 (February), 1–11. https://doi.org/10.3389/fmicb.2024.1308797.

Bolyen, E., Rideout, J.R., Dillon, M.R., Bokulich, N.A., Abnet, C.C., Al-Ghalith, G.A., Alexander, H., Alm, E.J., Arumugam, M., Asnicar, F., Bai, Y., Bisanz, J.E., Bittinger, K., Brejnrod, A., Brislawn, C.J., Brown, C.T., Callahan, B.J., Caraballo-Rodríguez, A.M., Chase, J., Caporaso, J.G., 2019. Reproducible, interactive, scalable and extensible microbiome data science using QIIME 2. In: Nature Biotechnology. Nat Biotechnol. https://doi.org/10.1038/s41587-019-0209-9, 37, Issue 8, pp. 852–857.

Bowles, M., Joye, S., 2011. High rates of denitrification and nitrate removal in cold seep sediments. ISME J. 5 (3), 565–567. https://doi.org/10.1038/ISMEJ.2010.134.

Callahan, B.J., McMurdie, P.J., Rosen, M.J., Han, A.W., Johnson, A.J.A., Holmes, S.P., 2016. DADA2: high-Resolution sample inference from illumina amplicon data. Nat. Methods 13 (7), 581–583. https://doi.org/10.1038/nmeth.3869.

Cánovas, C.R., Olías, M., Nieto, J.M., 2014. Metal(loid) attenuation processes in an extremely acidic river: the rio tinto (Sw Spain). Water Air Soil Pollut. 225 (1). https://doi.org/10.1007/s11270-013-1795-7.

Coleman, M.L., Hedrick, D.B., Lovley, D.R., White, D.C., Pye, K., 1993. Reduction of Fe (III) in sediments by sulphate-reducing bacteria. Nature 1993 361 (6411), 436–438. https://doi.org/10.1038/361436a0. *361*(6411).

Das, T., Chaudhury, G.R., Ayyappan, S., 1998. Use of Thiobacillus ferrooxidans for iron oxidation and precipitation. Biometals 11 (2), 125–129. https://doi.org/10.1023/A:1009277928506.

DI Tommaso, P., Chatzou, M., Floden, E.W., Barja, P.P., Palumbo, E., Notredame, C., 2017. Nextflow enables reproducible computational workflows. Nat. Biotechnol. 35 (4), 316–319. https://doi.org/10.1038/nbt.3820. Nat Biotechnol.

Diao, M., Dyksma, S., Koeksoy, E., Ngugi, D.K., Anantharaman, K., Loy, A., Pester, M., 2023. Global diversity and inferred ecophysiology of microorganisms with the potential for dissimilatory sulfate/sulfite reduction. FEMS (Fed. Eur. Microbiol. Soc.) Microbiol. Rev. 47 (5), 1–18. https://doi.org/10.1093/FEMSRE/FUAD058.

DiChristina, T.J., 1992. Effects of nitrate and nitrite on dissimilatory iron reduction by Shewanella putrefaciens 200. J. Bacteriol. 174 (6), 1891–1896. https://doi.org/10.1128/jb.174.6.1891-1896.1992.

Dobbin, P.S., Warren, L.H., Cook, N.J., McEwan, A.G., Powell, A.K., Richardson, D.J., 1996. Dissimilatory iron(III) reduction by Rhodobacter capsulatus. Microbiology (Reading, England) 142 (4), 765–774. https://doi.org/10.1099/00221287-142-4-765.

Dong, Y., Sanford, R.A., Boyanov, M.I., Flynn, T.M., O'Loughlin, E.J., Kemner, K.M., George, S., Fouke, K.E., Li, S., Huang, D., Li, S., Fouke, B.W., 2020. Controls on iron reduction and biomineralization over broad environmental conditions as suggested by the firmicutes Orenia metallireducens strain Z6. Environ. Sci. Technol. 54 (16), 10128–10140. https://doi.org/10.1021/acs.est.0c03853.

Estay, H., Barros, L., Troncoso, E., 2021. Metal sulfide precipitation: recent breakthroughs and future outlooks. Minerals 11 (12), 1385. https://doi.org/10.3390/MIN11121385, 2021, Vol. 11, Page 1385.

Ewels, P.A., Peltzer, A., Fillinger, S., Patel, H., Alneberg, J., Wilm, A., Garcia, M.U., Di Tommaso, P., Nahnsen, S., 2020. The nf-core framework for community-curated bioinformatics pipelines. In: Nature Biotechnology. Nature Publishing Group. https://doi.org/10.1038/s41587-020-0439-x, 38, Issue 3, pp. 276–278.

Falagán, C., Johnson, D.B., 2014. Acidibacter ferrireducens gen. Nov., sp. Nov.: an acidophilic ferric iron-reducing gammaproteobacterium. Extremophiles : Life under Extreme Conditions 18 (6), 1067–1073. https://doi.org/10.1007/S00792-014-0684-3.

Fernández-Remolar, D.C., Knoll, A.H., 2008. Fossilization potential of iron-bearing minerals in acidic environments of rio tinto, Spain: implications for Mars exploration. Icarus 194 (1), 72–85. https://doi.org/10.1016/J.ICARUS.2007.10.009.

Fernández-Remolar, D.C., Morris, R.V., Gruener, J.E., Amils, R., Knoll, A.H., 2005. The río tinto basin, Spain: mineralogy, sedimentary geobiology, and implications for interpretation of outcrop rocks at meridiani planum, Mars. Earth Planet Sci. Lett. 240 (1), 149–167. https://doi.org/10.1016/j.epsl.2005.09.043.

Finneran, K.T., Johnsen, C.V., Lovley, D.R., 2003. Rhodoferax ferrireducens sp. Nov., a psychrotolerant, facultatively anaerobic bacterium that oxidizes acetate with the reduction of Fe(III). Int. J. Syst. Evol. Microbiol. 53 (Pt 3), 669–673. https://doi.org/10.1099/IJS.0.02298-0.

Fredrickson, J.K., Zachara, J.M., Kennedy, D.W., Dong, H., Onstott, T.C., Hinman, N.W., Li, S.M., 1998. Biogenic iron mineralization accompanying the dissimilatory reduction of hydrous ferric oxide by a groundwater bacterium. Geochem. Cosmochim. Acta 62 (19–20), 3239–3257. https://doi.org/10.1016/S0016-7037(98)00243-9.

Fu, X., Hou, R., Yang, P., Qian, S., Feng, Z., Chen, Z., Wang, F., Yuan, R., Chen, H., Zhou, B., 2022. Application of external carbon source in heterotrophic denitrification of domestic sewage: a review. Sci. Total Environ. 817, 153061. https://doi.org/10.1016/j.scitotenv.2022.153061.

Giles, M., Morley, N., Baggs, E.M., Daniell, T.J., 2012. Soil nitrate reducing processes - drivers, mechanisms for spatial variation, and significance for nitrous oxide production. Front. Microbiol. 3. https://doi.org/10.3389/fmicb.2012.00407. DEC). Frontiers Media SA.

Glodowska, M., Stopelli, E., Schneider, M., Rathi, B., Straub, D., Lightfoot, A., Kipfer, R., Berg, M., Jetten, M., Kleindienst, S., Kappler, A., Glodowska, M., Kappler, A., Kleindienst, S., Cirpka, O.A., Rathi, B., Lightfoot, A., Stopelli, E., Berg, M., Prommer, H., 2020. Arsenic mobilization by anaerobic iron-dependent methane oxidation. Communications Earth & Environment 2020 1 (1), 1–7. https://doi.org/10.1038/s43247-020-00037-y, 1:1.

González-Toril, E., Llobet-Brossa, E., Casamayor, E.O., Amann, R., Amils, R., 2003. Microbial ecology of an extreme acidic environment, the tinto river. Appl. Environ. Microbiol. 69 (8), 4853–4865. https://doi.org/10.1128/AEM.69.8.4853-4865.2003.

Green, S.J., Prakash, O., Jasrotia, P., Overholt, W.A., Cardenas, E., Hubbard, D., Tiedje, J. M., Watson, D.B., Schadt, C.W., Brooks, S.C., Kostka, J.E., 2012. Denitrifying bacteria from the genus rhodanobacter dominate bacterial communities in the highly contaminated subsurface of a nuclear legacy waste site. Appl. Environ. Microbiol. 78 (4), 1039–1047. https://doi.org/10.1128/AEM.06435-11.

Hao, X., Zeng, W., Li, J., Zhan, M., Miao, H., Gong, Q., 2024. High-efficient nitrogen removal with low demand of Fe source and mechanism analysis driven by Fe(II)/Fe (III) cycle. Chem. Eng. J. 481. https://doi.org/10.1016/J.CEJ.2024.148702.

Hedrich, S., Schlömann, M., Barrie Johnson, D., 2011. The iron-oxidizing Proteobacteria. Microbiology 157 (6), 1551–1564. https://doi.org/10.1099/mic.0.045344-0. Microbiology (Reading).

Huang, Y.M., Straub, D., Blackwell, N., Kappler, A., Kleindienst, S., 2021. Meta-omics reveal gallionellaceae and rhodanobacter species as interdependent key players for Fe(II) oxidation and nitrate reduction in the autotrophic enrichment culture KS. Appl. Environ. Microbiol. 87 (15), 1–17. https://doi.org/10.1128/AEM.00496-21/SUPPL_FILE/AEM.00496-21-S0001. PDF.

Huang, J., Han, M., Yang, J., Kappler, A., Jiang, H., 2022a. Salinity Impact on Composition and Activity of Nitrate-Reducing Fe(II)-Oxidizing Microorganisms in Saline Lakes. Appl. Environ. Microbiol. 88 (10). https://doi.org/10.1128/aem.00132-22.

Huang, Y.M., Jakus, N., Straub, D., Konstantinidis, K.T., Blackwell, N., Kappler, A., Kleindienst, S., 2022b. "Candidatus ferrigenium straubiae" sp. nov., "Candidatus ferrigenium bremense" sp. nov., "Candidatus ferrigenium altingense" sp. Nov., are autotrophic Fe(II)-oxidizing bacteria of the family gallionellaceae. Syst. Appl. Microbiol. 45 (3). https://doi.org/10.1016/J.SYAPM.2022.126306.

Huang, Junjie, Gao, K., Yang, L., Lu, Y., 2023. Successional action of bacteroidota and firmicutes in decomposing straw polymers in a paddy soil. Environmental Microbiome 18 (1). https://doi.org/10.1186/s40793-023-00533-6.

Isobe, K., Ohte, N., 2014. Ecological perspectives on microbes involved in N-Cycling. Microb. Environ. 29 (1), 4. https://doi.org/10.1264/JSME2.ME13159.

Jain, A., Bonis, B.M., Gralnick, J.A., 2021. Oligo-heterotrophic activity of *Marinobacter subterrani* creates an indirect Fe(II)-oxidation phenotype in gradient tubes. Appl. Environ. Microbiol. https://doi.org/10.1128/AEM.01367-21.

Jakus, N., Blackwell, N., Osenbrück, K., Straub, D., Byrne, J.M., Wang, Z., Glöckler, D., Elsner, M., Lueders, T., Grathwohl, P., Kleindienst, S., Kappler, A., 2021. Nitrate Removal by a Novel Lithoautotrophic Nitrate-Reducing, Iron(II)-Oxidizing Culture Enriched from a Pyrite-Rich Limestone Aquifer. https://doi.org/10.1128/AEM.00460-21.

Jimenez-Castaneda, M.E., Scarinci, C., Burke, A., Boothman, C., Vaughan, D.J., Lloyd, J. R., van Dongen, B.E., 2020. Generation of alkalinity by stimulation of microbial iron reduction in acid rock drainage systems: impact of natural organic matter types. Water Air Soil Pollut. 231 (9). https://doi.org/10.1007/s11270-020-04820-7.

Kappler, Andreas, Bryce, C., 2017. Cryptic biogeochemical cycles: unravelling hidden redox reactions. Environ. Microbiol. 19 (3), 842–846. https://doi.org/10.1111/1462-2920.13687.

Kappler, A., Schink, B., Newman, D.K., 2005. Fe(III) mineral formation and cell encrustation by the nitrate-dependent Fe(II)-oxidizer strain BoFeN1. Geobiology 3 (4), 235–245. https://doi.org/10.1111/j.1472-4669.2006.00056.x.

Kelly, D.P., Wood, A.P., 2000. Confirmation of Thiobacillus denitrificans as a species of the genus Thiobacillus, in the β-subclass of the Proteobacteria, with strain NCIMB 9548 as the type strain. Int. J. Syst. Evol. Microbiol. 50 (2), 547–550. https://doi.org/10.1099/00207713-50-2-547.

Khaleque, H.N., González, C., Johnson, D.B., Kaksonen, A.H., Holmes, D.S., Watkin, E.L. J., 2020. Genome-based classification of Acidihalobacter prosperus f5 (=dsm 105917=jcm 32255) as Acidihalobacter yilgarnensis sp. Nov. Int. J. Syst. Evol. Microbiol. 70 (12), 6226–6234. https://doi.org/10.1099/ijsem.0.004519.

Klueglein, N., Kappler, A., 2013. Abiotic oxidation of Fe(II) by reactive nitrogen species in cultures of the nitrate-reducing Fe(II) oxidizer acidovorax sp. BoFeN1 - questioning the existence of enzymatic Fe(II) oxidation. Geobiology 11 (2), 180–190. https://doi.org/10.1111/gbi.12019.

Kontny, A., Schneider, M., Eiche, E., Stopelli, E., Glodowska, M., Rathi, B., Göttlicher, J., Byrne, J.M., Kappler, A., Berg, M., Thi, D.V., Trang, P.T.K., Viet, P.H., Neumann, T., 2021. Iron mineral transformations and their impact on as (im)mobilization at redox interfaces in As-contaminated aquifers. Geochem. Cosmochim. Acta 296, 189–209. https://doi.org/10.1016/J.GCA.2020.12.029.

Kurtzer, G.M., Sochat, V., Bauer, M.W., 2017. Singularity: scientific containers for mobility of compute. PLoS One 12 (5). https://doi.org/10.1371/journal.pone.0177459.

Küsel, K., Dorsch, T., Acker, G., Stackebrandt, E., 1999. Microbial reduction of Fe(III) in acidic sediments: isolation of Acidiphilium cryptum JF-5 capable of coupling the reduction of fe(III) to the oxidation of glucose. Appl. Environ. Microbiol. 65 (8), 3633–3640. https://doi.org/10.1128/aem.65.8.3633-3640.1999.

Laufer, Katja, Byrne, J.M., Glombitza, C., Schmidt, C., Jørgensen, B.B., Kappler, A., 2016a. Anaerobic microbial Fe(II) oxidation and Fe(III) reduction in coastal marine sediments controlled by organic carbon content. Environ. Microbiol. 18 (9), 3159–3174. https://doi.org/10.1111/1462-2920.13387.

Laufer, Katja, Røy, H., Jørgensen, B.B., Kappler, A., 2016b. Evidence for the existence of autotrophic nitrate-reducing Fe(II)-oxidizing bacteria in marine coastal sediment. Appl. Environ. Microbiol. 82 (20), 6120–6131. https://doi.org/10.1128/AEM.01570-16/SUPPL_FILE/ZAM999117455SO1.PDF.

Laufer, K., Nordhoff, M., Halama, M., Martinez, R.E., Obst, M., Nowak, M., Stryhanyuk, H., Richnow, H.H., Kappler, A., 2017. Microaerophilic Fe(II)-oxidizing Zetaproteobacteria isolated from low-Fe marine coastal sediments: physiology and

composition of their twisted stalks. Appl. Environ. Microbiol. 83 (8). https://doi.org/10.1128/AEM.03118-16.
Lentini, C.J., Wankel, S.D., Hansel, C.M., 2012. Enriched iron(III)-reducing bacterial communities are shaped by carbon substrate and iron oxide mineralogy. Front. Microbiol. 3 (DEC), 1–19. https://doi.org/10.3389/fmicb.2012.00404.
Li, N., Li, Y., Lou, R., Xu, H., Saeed, L., 2023. Effects of Fe(II) and organic carbon on nitrate reduction in surficial sediments of a large shallow freshwater Lake. J. Environ. Manag. 336, 117623. https://doi.org/10.1016/J.JENVMAN.2023.117623.
López-Archilla, A.I., Marin, I., Amils, R., 2001. Microbial community composition and ecology of an acidic aquatic environment: the tinto river, Spain. Microb. Ecol. 41 (1), 20–35. https://doi.org/10.1007/s002480000044.
Lovley, D.R., 1987. Organic matter mineralization with the reduction of ferric iron: a review. Geomicrobiol. J. 5 (3–4), 375–399. https://doi.org/10.1080/01490458709385975.
Lueders, T., Manefield, M., Friedrich, M.W., 2004. Enhanced sensitivity of DNA- and rRNA-based stable isotope probing by fractionation and quantitative analysis of isopycnic centrifugation gradients. Environ. Microbiol. 6 (1), 73–78. https://doi.org/10.1046/j.1462-2920.2003.00536.x.
Luptáková, A., Kotuličová, I., Bálintová, M., Demčák, Š., 2015. Bacterial reduction of barium sulphate by sulphate-reducing bacteria. Nova Biotechnologica et Chimica 14 (2), 135–140. https://doi.org/10.1515/nbec-2015-0022.
Mansor, M., Drabesch, S., Bayer, T., Van Le, A., Chauhan, A., Schmidtmann, J., Peiffer, S., Kappler, A., 2021. Application of single-particle ICP-MS to determine the mass distribution and number concentrations of environmental nanoparticles and colloids. Environ. Sci. Technol. Lett. 8 (7), 589–595. https://doi.org/10.1021/acs.estlett.1c00314.
Martin, M., 2011. Cutadapt removes adapter sequences from high-throughput sequencing reads. EMBnet.Journal 17 (1), 10. https://doi.org/10.14806/ej.17.1.200.
McAllister, S.M., Vandzura, R., Keffer, J.L., Polson, S.W., Chan, C.S., 2021. Aerobic and anaerobic iron oxidizers together drive denitrification and carbon cycling at marine iron-rich hydrothermal vents. ISME J. 15 (5), 1271–1286. https://doi.org/10.1038/S41396-020-00849-Y.
M.dos, S., Stumm, W., 1992. Reductive dissolution of Iron(III) (hydr)oxides by hydrogen sulfide. Langmuir 8 (6), 1671–1675. https://doi.org/10.1021/la00042a030.
Moeslundi, L., Thamdrup, B., Barker Jørgensen, B., 1994. Sulfur and iron cycling in a coastal sediment: radiotracer studies and seasonal dynamics. Biogeochemistry 27 (2), 129–152. https://doi.org/10.1007/BF00002815.
Mortimer, R.J.G., Harris, S.J., Krom, M.D., Freitag, T.E., Prosser, J.I., Barnes, J., Anschutz, P., Hayes, P.J., Davies, I.M., 2004. Anoxic nitrification in marine sediments. Mar. Ecol. Prog. Ser. 276 (1), 37–51. https://doi.org/10.3354/MEPS276037.
Moya-Beltrán, A., Beard, S., Rojas-Villalobos, C., Issotta, F., Gallardo, Y., Ulloa, R., Giaveno, A., Degli Esposti, M., Johnson, D.B., Quatrini, R., 2021. Genomic evolution of the class acidithiobacillia: deep-branching proteobacteria living in extreme acidic conditions. ISME J. 15 (11), 3221–3238. https://doi.org/10.1038/s41396-021-00995-x.
Muehe, E.M., Gerhardt, S., Schink, B., Kappler, A., 2009. Ecophysiology and the energetic benefit of mixotrophic Fe(II) oxidation by various strains of nitrate-reducing bacteria. FEMS (Fed. Eur. Microbiol. Soc.) Microbiol. Ecol. 70 (3), 335–343. https://doi.org/10.1111/j.1574-6941.2009.00755.x.
Neil, C.W., Ray, J.R., Lee, B., Jun, Y.S., 2016. Fractal aggregation and disaggregation of newly formed iron(III) (hydr)oxide nanoparticles in the presence of natural organic matter and arsenic. Environ. Sci. Nano 3 (3), 647–656. https://doi.org/10.1039/c5en00283d.
Nielsen, J.L., Nielsen, P.H., 1998. Microbial nitrate-dependent oxidation of ferrous iron in activated sludge. Environ. Sci. Technol. 32 (22), 3556–3561. https://doi.org/10.1021/es9803299.
Olías, M., Nieto, J.M., 2015. Background conditions and mining pollution throughout history in the río tinto (SW Spain). Environments - MDPI 2 (3), 295–316. https://doi.org/10.3390/environments2030295.
Olías, M., Cánovas, C.R., Macías, F., Basallote, M.D., Nieto, J.M., 2020. The evolution of pollutant concentrations in a river severely affected by acid mine drainage: río tinto (SW Spain). Minerals 10 (7), 598. https://doi.org/10.3390/MIN10070598, 2020, Vol. 10, Page 598.
Otte, J.M., Blackwell, N., Soos, V., Rughöft, S., Maisch, M., Kappler, A., Kleindienst, S., Schmidt, C., 2018. Sterilization impacts on marine sediment-are we able to inactivate microorganisms in environmental samples? FEMS (Fed. Eur. Microbiol. Soc.) Microbiol. Ecol. 94 (12), 1–14. https://doi.org/10.1093/femsec/fiy189.
O'loughlin, E.J., Boyanov, M.I., Gorski, C.A., Scherer, M.M., Kemner, K.M., 2021. Effects of Fe(III) oxide mineralogy and phosphate on Fe(II) secondary mineral formation during microbial iron reduction. Minerals 11 (2), 1–43. https://doi.org/10.3390/MIN11020149.
Pan, B., Xia, L., Lam, S.K., Wang, E., Zhang, Y., Mosier, A., Chen, D., 2022. A global synthesis of soil denitrification: driving factors and mitigation strategies. Agric. Ecosyst. Environ. 327, 107850. https://doi.org/10.1016/J.AGEE.2021.107850.
Pantke, C., Obst, M., Benzerara, K., Morin, G., Ona-Nguema, G., Dippon, U., Kappler, A., 2012. Green rust formation during Fe(II) oxidation by the nitrate-reducing acidovorax sp. strain BoFeN1. Environ. Sci. Technol. 46 (3), 1439–1446. https://doi.org/10.1021/es2016457.
Parada, A.E., Needham, D.M., Fuhrman, J.A., 2016. Every base matters: assessing small subunit rRNA primers for marine microbiomes with mock communities, time series and global field samples. Environ. Microbiol. 18 (5), 1403–1414. https://doi.org/10.1111/1462-2920.13023.
Patzner, M.S., Mueller, C.W., Malusova, M., Baur, M., Nikeleit, V., Scholten, T., Hoeschen, C., Byrne, J.M., Borch, T., Kappler, A., Bryce, C., 2020. Iron mineral dissolution releases iron and associated organic carbon during permafrost thaw. Nat. Commun. (1), 1–11. https://doi.org/10.1038/s41467-020-20102-6, 2020 11:1, 11.
Peiffer, S., Walton-Day, K., Macalady, D.L., 1999. The interaction of natural organic matter with iron in a wetland (tennessee park, Colorado) receiving acid mine drainage. Aquat. Geochem. 5 (2), 207–223. https://doi.org/10.1023/A:1009617925959.
Peng, C., Bryce, C., Sundman, A., Kappler, A., 2019. Cryptic cycling of complexes containing Fe(III) and organic matter by phototrophic Fe(II)-oxidizing bacteria. Appl. Environ. Microbiol. 85 (8). https://doi.org/10.1128/AEM.02826-18.
Porsch, K., Kappler, A., 2011. FeII oxidation by molecular O2 during HCl extraction. Environ. Chem. 8 (2), 190–197. https://doi.org/10.1071/EN10125.
Poulain, A.J., Newman, D.K., 2009. Rhodobacter capsulatus catalyzes light-dependent Fe (II) oxidation under anaerobic conditions as a potential detoxification mechanism. Appl. Environ. Microbiol. 75 (21), 6639–6646. https://doi.org/10.1128/AEM.00054-09.
Quast, C., Pruesse, E., Yilmaz, P., Gerken, J., Schweer, T., Yarza, P., Peplies, J., Glöckner, F.O., 2013. The SILVA ribosomal RNA gene database project: improved data processing and web-based tools. Nucleic Acids Res. 41 (D1). https://doi.org/10.1093/nar/gks1219.
Ravel, B., Newville, M., 2005. ATHENA, artemis, hephaestus: data analysis for X-ray absorption spectroscopy using IFEFFIT. J. Synchrotron Radiat. 12 (4), 537–541. https://doi.org/10.1107/S0909049505012719.
Reyes, C., Dellwig, O., Dähnke, K., Gehre, M., Noriega-Ortega, B.E., Böttcher, M.E., Meister, P., Friedrich, M.W., 2016. Bacterial communities potentially involved in iron-cycling in Baltic sea and north sea sediments revealed by pyrosequencing. FEMS (Fed. Eur. Microbiol. Soc.) Microbiol. Ecol. 92 (4), 1–14. https://doi.org/10.1093/femsec/fiw054.
Roden, E.E., Zachara, J.M., 1996. Microbial reduction of crystalline Iron(III) oxides: influence of oxide surface area and potential for cell growth. Cell Growth 214. https://digitalcommons.unl.edu/usdoepubhttps://digitalcommons.unl.edu/usdoepub/214.
Sánchez-Andrea, I., Rodríguez, N., Amils, R., Sanz, J.L., 2011. Microbial diversity in anaerobic sediments at río tinto, a naturally acidic environment with a high heavy metal content. Appl. Environ. Microbiol. 77 (17), 6085–6093. https://doi.org/10.1128/AEM.00654-11.
Sánchez-Andrea, I., Knittel, K., Amann, R., Amils, R., Sanz, J.L., 2012. Quantification of tinto river sediment microbial communities: importance of sulfate-reducing bacteria and their role in attenuating acid mine drainage. Appl. Environ. Microbiol. 78 (13), 4638–4645. https://doi.org/10.1128/AEM.00848-12.
Schaedler, F., Kappler, A., Schmidt, C., 2018. A revised iron extraction protocol for environmental samples rich in nitrite and carbonate. Geomicrobiol. J. 35 (1), 23–30. https://doi.org/10.1080/01490451.2017.1303554.
Schalk, I.J., Perraud, Q., 2023. Pseudomonas aeruginosa and its multiple strategies to access iron. In: Environmental Microbiology. John Wiley & Sons, Ltd. https://doi.org/10.1111/1462-2920.16328, 25, Issue 4, pp. 811–831.
Smith, R.L., Kent, D.B., Repert, D.A., Böhlke, J.K., 2017. Anoxic nitrate reduction coupled with iron oxidation and attenuation of dissolved arsenic and phosphate in a sand and gravel aquifer. Geochem. Cosmochim. Acta 196, 102–120. https://doi.org/10.1016/J.GCA.2016.09.025.
Sobron, P., Bishop, J.L., Blake, D.F., Chen, B., Rull, F., 2014. Natural Fe-bearing oxides and sulfates from the rio tinto Mars analog site: critical assessment of VNIR reflectance spectroscopy, laser raman spectroscopy, and XRD as mineral identification tools. Am. Mineral. 99 (7), 1199–1205. https://doi.org/10.2138/AM.2014.4595/MACHINEREADABLECITATION/RIS.
Stookey, L.L., 1970. Ferrozine-A new spectrophotometric reagent for iron. Anal. Chem. 42 (7), 779–781. https://doi.org/10.1021/ac60289a016.
Straub, K.L., Benz, M., Schink, B., Widdel, F., 1996. Anaerobic, nitrate-dependent microbial oxidation of ferrous iron. Appl. Environ. Microbiol. 62 (4), 1458–1460. https://doi.org/10.1128/aem.62.4.1458-1460.1996.
Straub, K.L., Schönhuber, W.A., Buchholz-Cleven, B.E.E., Schink, B., 2004. Diversity of ferrous iron-oxidizing, nitrate-reducing bacteria and their involvement in oxygen-independent iron cycling. Geomicrobiol. J. 21 (6), 371–378. https://doi.org/10.1080/01490450490485854.
Straub, D., Blackwell, N., Langarica-Fuentes, A., Peltzer, A., Nahnsen, S., Kleindienst, S., 2020. Interpretations of environmental microbial community studies are biased by the selected 16S rRNA (gene) amplicon sequencing pipeline. Front. Microbiol. 11, 550420. https://doi.org/10.3389/FMICB.2020.550420/BIBTEX.
Stumm, W., Morgan, J.J., 1996. Aquatic chemistry: Chemical equilibria and rates. In: natural waters, 3rd ed. Wiley-Interscience.
Sun, K., Yu, M., Zhu, X.-Y., Xue, C.-X., Zhang, Y., Chen, X., Yao, P., Chen, L., Fu, L., Yang, Z., Zhang, X.-H., 2023. Microbial communities related to the sulfur cycle in the sansha yongle blue hole. Microbiol. Spectr. 11 (5). https://doi.org/10.1128/spectrum.01149-23.
Tang, Z., Chen, · Lin, Zhang, Y., Xia, M., Zhou, Z., Wang, Q., Taoli, H., Zheng, T., Meng, · Xiaoshan, 2010. Improved Short-Chain Fatty Acids Production and Protein Degradation During the Anaerobic Fermentation of Waste-Activated Sludge via Alumina Slag-Modified Biochar. https://doi.org/10.1007/s12010-023-04816-z.
Tiedje, J., 1988. Ecology of denitrification and dissimilatory nitrate reduction to ammonium - tiedje. Methods of Soil Analysis. Part 2. Chemical and Microbiological Properties 717 papers://27281f87-3b7a-4de6-820c-ad3b64393d15/Paper/p.3339.
Tong, H., Li, J., Chen, M., Fang, Y., Yi, X., Dong, L., Jiang, Q., Liu, C., 2023. Iron oxidation coupled with nitrate reduction affects the acetate-assimilating microbial community structure elucidated by stable isotope probing in flooded paddy soil. Soil Biol. Biochem. 183, 109059. https://doi.org/10.1016/j.soilbio.2023.109059.

Tor, J.M., Kashefi, K., Lovley, D.R., 2001. Acetate oxidation coupled to Fe(III) reduction in hyperthermophilic microorganisms. Appl. Environ. Microbiol. 67 (3), 1363–1365. https://doi.org/10.1128/AEM.67.3.1363-1365.2001.

van den Berg, E.M., Boleij, M., Kuenen, J.G., Kleerebezem, R., van Loosdrecht, M.C.M., 2016. DNRA and denitrification coexist over a broad range of acetate/N-NO3- ratios, in a chemostat enrichment culture. Front. Microbiol. 7 (NOV), 224494. https://doi.org/10.3389/fmicb.2016.01842.

Vera, M., Schippers, A., Sand, W., 2013. Progress in bioleaching: fundamentals and mechanisms of bacterial metal sulfide oxidation-part A. Appl. Microbiol. Biotechnol. 97 (17), 7529–7541. https://doi.org/10.1007/s00253-013-4954-2.

Wang, G., Tang, K., Yao, Y., Zhang, W., Angela, Andersen, H.R., Zhang, Y., 2023. Improved Fe(II) regeneration from actual ferric sludge using a biocathode with granular sludge. J. Clean. Prod. 389. https://doi.org/10.1016/J.JCLEPRO.2023.136118.

Wissuwa, J., Bauer, S.L.M., Steen, I.H., Stokke, R., 2017. Complete genome sequence of Lutibacter profundi LP1T isolated from an Arctic deep-sea hydrothermal vent system. Stand. Genomic Sci. 12 (1). https://doi.org/10.1186/S40793-016-0219-X.

Xie, L., Yoshida, N., Meng, L., 2023. Polyphasic characterization of geotalea uranireducens NIT-SL11 newly isolated from a complex of sewage sludge and microbially reduced graphene oxide. Microorganisms 11 (2), 349. https://doi.org/10.3390/MICROORGANISMS11020349, 2023, Vol. 11, Page 349.

Xiu, W., Yu, X., Guo, H., Yuan, W., Ke, T., Liu, G., Tao, J., Hou, W., Dong, H., 2019. Facilitated arsenic immobilization by biogenic ferrihydrite-goethite biphasic Fe(III) minerals (Fh-Gt bio-bi-minerals). Chemosphere 225, 755–764. https://doi.org/10.1016/J.CHEMOSPHERE.2019.02.098.

Yuan, C., Fitzpatrick, R., Mosley, L.M., Marschner, P., 2015. Sulfate reduction in sulfuric material after re-flooding: effectiveness of organic carbon addition and pH increase depends on soil properties. J. Hazard Mater. 298, 138–145. https://doi.org/10.1016/j.jhazmat.2015.05.013.

Zhang, S.H., Cai, L.L., Liu, Y., Shi, Y., Li, W., 2009. Effects of NO2(-) and NO3(-) on the Fe (III)EDTA reduction in a chemical absorption-biological reduction integrated NO(x) removal system. Appl. Microbiol. Biotechnol. 82 (3), 557–563. https://doi.org/10.1007/S00253-008-1837-Z.

Zhang, L., Zeng, Q., Liu, X., Chen, P., Guo, X., Ma, L.Z., Dong, H., Huang, Y., 2019. Iron reduction by diverse actinobacteria under oxic and pH-neutral conditions and the formation of secondary minerals. Chem. Geol. 525, 390–399. https://doi.org/10.1016/J.CHEMGEO.2019.07.038.

Zhu, E., Liu, T., Zhou, L., Wang, S., Wang, X., Zhang, Z., Wang, Z., Bai, Y., Feng, X., 2020. Leaching of organic carbon from grassland soils under anaerobiosis. Soil Biol. Biochem. 141. https://doi.org/10.1016/J.SOILBIO.2019.107684.